VOF BASED MULTIPHASE LATTICE BOLTZMANN METHOD USING EXPLICIT KINEMATIC BOUNDARY CONDITONS AT THE INTERFACE

A Thesis
Presented to
The Academic Faculty

by

Deepak Maini

In Partial Fulfillment
of the Requirements for the Degree
Master of Science in the
School of Mechanical Engineering/Paper Science and Engineering

Georgia Institute of Technology
August 2007

VOF BASED MULTIPHASE LATTICE BOLTZMANN METHOD USING EXPLICIT KINEMATIC BOUNDARY CONDITONS AT THE INTERFACE

Approved by:

Dr. Cyrus Aidun, Advisor
School of Mechanical Engineering
Georgia Institute of Technology

Dr. Minami Yoda
School of Mechanical Engineering
Georgia Institute of Technology

Dr. S.M. Ghiaasiaan
School of Mechanical Engineering
Georgia Institute of Technology

Date Approved: June 6, 2007

To mum and dad

ACKNOWLEDGEMENTS

I want to thank my advisor, Dr. Cyrus Aidun, for being my mentor and helping me at every step toward completion of my Master's thesis. It has been my honor to work under him and successfully complete my MS degree.

Thanks to Dr. Minami Yoda and Dr. S.M. Ghiaasiaan for helping me understand complex phenomena related to my research.

Special thanks to all the graduate students working in my lab at the Institute of Paper Science and Technology for their help and support.

Finally, I would like to thank my parents for believing in me and supporting me at every step from my childhood to this day.

TABLE OF CONTENTS

LIST OF TABLES

LIST OF FIGURES

LIST OF SYMBOLS AND ABBREVIATIONS

Symbols

λ .....wavelength

f.....single particle distribution function

Ω ……..collision operator

k.……...…phase

k' ……..other phase

τ ……*relaxation parameter*

ρ ……..density

$\vec{x}$ …….....position vector

$\vec{e}_i$ ……..link velocity vector

t.……time

$\vec{v}$ …….…..velocity vector

$\vec{F}$ ……...local color gradient

$\vec{j}$ ……...local color momentum

V …….….interaction pseudo-potential

G …….strength of interaction

ψ ……..function of density

Ψ …….free-energy functional

VOF ……....volume-of-fluid

c ……...*lattice speed*

w …...……..weight function

r …….....density ratio

g ……...…...body-force

$\vec{g}$ ……..body-force vector

p ……..pressure

σ ……..surface tension

K …….curvature

μ ……..kinematic viscosity

$\vec{n}$ ……..normal vector at the interface

c_s …….….pseudo-sound-speed

$\vec{S}$ ……..normal-stress jump vector

Vsp ……spurious velocity

R ……..radius of curvature

Ca ……....capillary number

M ……density ratio

m …….lattice-spacing ratio

Re ……Reynolds number

Subscripts

i ……...link ‘i’

k ……..phase

r ……...red

b ……..blue

kk' ……between two phases

α ……alpha fluid

β ……..beta fluid

1 ……..x-direction

2 ……..y-direction

c ……..coarse grid

f ……fine grid

Superscripts

k ……..phase

k' ……..other phase

r ……...red

b ……..blue

α ……alpha fluid

β ……..beta fluid

eq …….equilibrium

c ……..coarse grid

f ……fine grid

SUMMARY

A Volume-of-Fluid (VOF) based multiphase Lattice Boltzmann method that explicitly prescribes kinematic boundary conditions at the interface is developed. The advantage of the method is the direct control over the surface tension value. The details of the numerical method are presented. The Saffman instability, Taylor instability, and flow of deformable suspensions in a channel are used as example-problems to demonstrate the accuracy of the method. The method allows for relatively large viscosity and density ratios.

The method discussed in the present study aims at resolving the interface precisely using the VOF concept in background of the Gunstensen's method. The basic ideas of the Gunstensen's method are used, but with some fundamental improvements. Surface tension, which is implicitly provided in the Gunstensen's method, is explicitly supplied in the present method. The present method also takes normal stress into account to describe the interfacial dynamics. It can handle considerably high density and viscosity ratios for incompressible flows.

Chapter 1

Introduction

In recent years, the lattice Boltzmann method (LBM) has developed into an alternative and promising numerical scheme for simulating fluid flows and modeling physics in fluids. The scheme is particularly successful in fluid flow applications involving interfacial dynamics and complex boundaries. Unlike conventional numerical schemes based on discretizations of macroscopic continuum equations, the lattice Boltzmann method is based on microscopic models and mesoscopic kinetic equations. The fundamental idea of the LBM is to construct simplified kinetic models that incorporate the essential physics of microscopic or mesoscopic processes so that the macroscopic averaged properties obey the desired macroscopic equations. The basic premise for using these simplified kinetic-type methods for macroscopic fluid flows is that the macroscopic dynamics of a fluid are the result of the collective behavior of many microscopic particles in the system and that the macroscopic dynamics are not sensitive to the underlying details in macroscopic physics. By developing a simplified version of the kinetic equation, one avoids complicated kinetic equations such as the full Boltzmann equation, and one avoids following each particle as in molecular dynamics simulations.

Even though the LBM is based on a particle picture, its principal focus is the averaged macroscopic behavior. The kinetic equation provides many of the advantages of molecular dynamics, including clear physical pictures, easy implementation of boundary conditions, and fully parallel algorithms. Because of the availability of very fast and

massively parallel machines, there is a current trend to use codes that can exploit the intrinsic features of parallelism. The LBM fulfills these requirements in a straightforward manner.

The kinetic nature of the LBM introduces three important features that distinguish it from other numerical methods. First, the convection operator (or the streaming process in the LBM) of the LBM in phase space (or velocity space) is linear. This feature is borrowed from kinetic theory and contrasts with the nonlinear convection terms in other approaches that use a macroscopic representation. Simple convection combined with a relaxation process (or collision operator in the LBM, which is same as viscous diffusion in the Navier-Stokes equations) allows the recovery of the non-linear macroscopic advection through multi-scale expansions. Second, the incompressible Navier-Stokes (NS) equations can be obtained in the nearly incompressible limit of the LBM. The pressure of the LBM is calculated using an equation of state (like the ideal-gas equation). In contrast, in the direct numerical simulation of the incompressible NS equations, the pressure satisfies a Poisson equation with velocity strains acting as sources. Solving this equation for the pressure often produces numerical difficulties requiring special treatment, such as iteration or relaxation. Third, the LBM utilizes a minimal set of velocities in phase space. In the traditional kinetic theory with the Maxwell-Boltzmann equilibrium distribution, the phase space is a complete functional space. The averaging process involves information from the whole velocity phase space. Because only one or two speeds and a few moving directions are in the LBM, the transformation relating the microscopic distribution

function and macroscopic quantities is greatly simplified and consists of simple arithmetic calculations.

The LBM originated from lattice gas (LG) automata, a discrete particle kinetics utilizing a discrete lattice and discrete time. The LBM can also be viewed as a special finite difference scheme for the kinetic equation of the discrete-velocity distribution function. The idea of using the simplified kinetic equation with a single-particle speed to simulate fluid flows was employed by Broadwell (1964) for studying shock structures. In fact, one can view the Broadwell model as a simple one-dimensional lattice Boltzmann equation. Multispeed discrete particle velocities models have also been used for studying shock-wave structure, by Inamuro & Sturtevant (1990), for example. In all these models, although the particle velocity in the distribution function was discretized, space and time were continuous. The full discrete particle velocity model, where space and time are also discretized on a square lattice, was proposed by Hardy et al (1976) for studying transport properties of fluids. In their seminal work on the lattice gas automaton method for two-dimensional hydrodynamics, Frisch et al. (1986) recognized the importance of the symmetry of the lattice for the recovery of the NS equations obtaining for the first time the correct NS equations starting from lattice gas automata on a hexagonal lattice. The central ideas in the papers contemporary with the FHP paper include the cellular automaton model (Wolfram 1996) and the 3-D model using the four-dimensional face-centered-hyper-cubic (FCHC) lattice.

The lattice gas automaton is constructed as a simplified, fictitious molecular dynamic in which space, time, and particle velocities are all discrete. From this perspective, the lattice gas method is often called the lattice gas cellular automata technique. In general, a lattice gas automaton consists of a regular lattice with particles residing on the nodes. A set of Boolean variables $n_i(\vec{x},t)$ (i=1,……, M) describing the particle occupation is defined, where M is the number of directions of the particle velocities at each node. The evolution equation of the LG automata is as follows:

$$n_i(\vec{x}+\vec{e}_i,t+1) = n_i(\vec{x},t) + \Omega_i(n(\vec{x},t)) \qquad \text{(i=1,….., M)} \qquad (1)$$

where $\vec{e}_i$ are the local particle velocities. Starting from an initial state, the configuration of particles at each time step evolves in two sequential sub-steps: (a) streaming, in which each particle moves to the nearest node in the direction of its velocity, and (b) collision, which occurs when particles arriving at a node interact and change their velocity directions according to scattering rules. For simplicity, the exclusion rule (no more than one particle being allowed at a given time and node with a given velocity) is imposed for memory efficiency and leads to a Fermi-Dirac local equilibrium distribution.

The main feature of the LBM is to replace the particle occupation variables, $n_i(\vec{x},t)$ (Boolean variables), in equation (1), by single-particle distribution functions (real variables) $f_i = \langle n_i \rangle$ and neglect individual particle motion and particle-particle correlations in the kinetic equations (McNamara & Zanetti 1988), where < > denotes an ensemble average. This procedure eliminates statistical noise in the LBM. In the LBM, the primitive variables are the averaged particle distributions, which are mesoscopic

variables. Because the kinetic form is still the same as the LG automata, the advantages of locality in the kinetic approach are retained. The locality is essential to parallelism.

An important simplification was made by Higuera & Jimenez (1989) who linearized the collision operator by assuming that the distribution is close to the local equilibrium state. An enhanced collision operator approach, which is linearly stable, was proposed by Higuera et al (1989). A particularly simple linearized version of the collision operator makes use of a relaxation time toward the local equilibrium using a single time relaxation. The relaxation term is known as the Bhatnagar-Gross,-Krook (BGK) collision operator (Bhatnagar et al 1954) and has been independently suggested by several authors. In this lattice BGK (LBGK) model, the local equilibrium distribution is chosen to recover the NS macroscopic equations (Qian et al 1992, Chen et al 1992). Use of the lattice BGK model makes the computations more efficient and allows flexibility of the transport coefficients.

LBE: An extension of LG Automata

There are several ways to obtain the lattice Boltzmann equation (LBE) from either discrete velocity models or the Boltzmann kinetic equation. There are also several ways to derive the macroscopic Navier-Stokes (NS) equations from the LBE. Because the LBM is a derivative of the LG method, the LBE is introduced starting from a discrete kinetic equation for the particle distribution function, which is similar to the kinetic equation in the LG automata in equation (1):

$$f_i(\vec{x} + \vec{e}_i \Delta x, t + \Delta t) = f_i(\vec{x}, t) + \Omega_i(f(\vec{x}, t)) \qquad (i=1,\ldots\ldots, M) \qquad (2)$$

where f_i is the particle velocity distribution function along the i[th] direction; $\Omega_i = \Omega_i(f)$ is the collision operator which represents the rate of change of f_i resulting from collision, and Δt and Δx are time and space increments, respectively. When $\Delta x / \Delta t = |\vec{e}_i|$, equations (1) and (2) have the same discretizations. Ω_i depends only on the local distribution function. In the LBM, space is discretized in a way that is consistent with the kinetic equations, i.e. the coordinates of the nearest neighbor points around $\vec{x}$ are $\vec{x} + \vec{e}_i$. The density ρ and the momentum density $\rho \vec{v}$ are defined as particle velocity moments of the distribution function, f_i,

$$\begin{aligned} \rho &= \sum_i f_i \\ \rho \vec{v} &= \sum_i f_i \vec{e}_i \end{aligned} \tag{3}$$

Ω_i is required to satisfy conservation of total mass and total momentum at each lattice:

$$\begin{aligned} \sum_i \Omega_i &= 0 \\ \sum_i \Omega_i \vec{e}_i &= 0 \end{aligned} \tag{4}$$

If only the physics in the long wave-length and low-frequency limit are of interest, the lattice spacing Δx and the time increment Δt in equation (2) can be regarded as small parameters of the same order ε. Performing a Taylor expansion in time and space, the following continuum form of the kinetic equation accurate to second order in ε is obtained:

$$\frac{\partial f_i}{\partial t} + \vec{e}_i . \nabla f_i + \varepsilon \left(\frac{1}{2} \vec{e}_i \vec{e}_i : \nabla \nabla f_i + e_i \cdot \nabla \frac{\partial f_i}{\partial t} + \frac{1}{2} \frac{\partial^2 f_i}{\partial t^2} \right) = \frac{\Omega_i}{\varepsilon} \tag{5}$$

To derive the macroscopic hydrodynamic equation, the Chapman-Enskog expansion, which is essentially a formal multiscaling expansion, is used:

$$\left[\frac{\partial}{\partial t} = \varepsilon \frac{\partial}{\partial t_1} + \varepsilon^2 \frac{\partial}{\partial t_2} , \qquad \frac{\partial}{\partial x} = \varepsilon \frac{\partial}{\partial x_1} \right]$$

The above formula assumes that the diffusion time scale t_2 is much slower than the convection time scale t_1. Likewise, the one-particle distribution f_i can be expanded formally about the local equilibrium distribution function f_i^{eq},

$$f_i = f_i^{(neq)} + f_i^{eq} \tag{6}$$

Here f_i^{eq} depends on the local macroscopic variables (ρ and $\rho \vec{\mathrm{v}}$) and should satisfy the following constraints:

$$\begin{aligned} \sum_i f_i^{eq} &= \rho \\ \sum_i f_i^{eq} \vec{\mathrm{e}}_i &= \rho \vec{\mathrm{v}} \end{aligned} \tag{7}$$

$f_i^{(neq)} = f_i^{(1)} + \varepsilon f_i^{(2)} + O(\varepsilon^2)$ is the nonequilibrium distribution function, which has the following constraints:

$$\begin{aligned} \sum_i f_i^{(k)} &= 0 \\ \sum_i f_i^{(k)} \vec{\mathrm{e}}_i &= 0 \end{aligned} \tag{8}$$

for both k=1 and k=2.

Inserting f_i into the collision operator Ω_i, the Taylor expansion gives:

$$\Omega_i(f) = \Omega_i(f^{eq}) + \varepsilon \frac{\partial \Omega_i(f^{eq})}{\partial f_j} f_j^{(1)} + \varepsilon^2 \left(\frac{\partial \Omega_i(f^{eq})}{\partial f_j} f_j^{(2)} + \frac{\partial^2 \Omega_i(f^{eq})}{\partial f_j \partial f_k} f_j^{(1)} f_k^{(1)} \right) + O(\varepsilon^3) \tag{9}$$

From equation (5) when $\varepsilon \to 0$, $\Omega_i(f^{eq}) = 0$. This leads to a linearized collision operator,

$$\frac{\Omega_i(f)}{\varepsilon} = \frac{M_{ij}}{\varepsilon}(f_j - f_j^{eq}), \tag{10}$$

where $M_{ij} = \frac{\partial \Omega_i(f^{eq})}{\partial f_j}$ is the collision matrix (Higuera & Jimenez 1989), which determines the scattering rate between directions *i* and *j*. For a given lattice, M_{ij} only depends on the angle between directions *i* and *j* and has a limited set of values. For mass and momentum conservation collision, M_{ij} satisfy the following constaints:

$$\begin{aligned} &\sum_i M_{ij} = 0 \\ &\sum_i M_{ij}\vec{\mathrm{e}}_i = 0 \end{aligned} \tag{11}$$

If another assumption that the local particle distribution relaxes to an equilibrium state at a single rate τ is made,

$$M_{ij} = -\frac{1}{\tau}\delta_{ij} \tag{12}$$

the lattice Boltzmann collision term is obtained,

$$\frac{\Omega_i}{\varepsilon} = -\frac{1}{\tau} f_i^{neq} = -\frac{1}{\varepsilon\tau}\left(f_i^{(1)} + \varepsilon f_i^{(2)}\right), \tag{13}$$

and the LBGK equation:

$$f_i(\vec{\mathrm{x}} + \vec{\mathrm{e}}_i\Delta t, t + \Delta t) = f_i(\vec{\mathrm{x}}, t) - \frac{f_i(\vec{\mathrm{x}}, t) - f_i^{eq}(\vec{\mathrm{x}}, t)}{\tau} \tag{14}$$

From equation (5) one obtains the following equations:

$$\frac{\partial f_i^{eq}}{\partial t_1} + \vec{\mathrm{e}}_i \cdot \nabla_1 f_i^{eq} = -\frac{f_i^{(1)}}{\tau} \tag{15}$$

To order ε^0 and

$$\frac{\partial}{\partial t_1} f_i^{(1)} + \frac{\partial}{\partial t_2} f_i^{eq} + \vec{e}_i \cdot \nabla f_i^{(1)} + \frac{1}{2}\vec{e}_i\vec{e}_i : \nabla\nabla f_i^{eq} + \vec{e}_i \cdot \nabla \frac{\partial}{\partial t_1} f_i^{eq} + \frac{1}{2}\frac{\partial^2}{\partial t_1^2} f_i^{eq} = \frac{1}{\tau} f_i^{(2)} \quad (16)$$

to order ε^1. Using equation (15) and some algebra, we can rewrite the first order equation as

$$\frac{\partial f_i^{(1)}}{\partial t_2} + \left(1 - \frac{2}{\tau}\right)\left[\frac{\partial f_i^{(1)}}{\partial t_1} + \vec{e}_i \cdot \nabla_1 f_i^{(1)}\right] = -\frac{f_i^{(2)}}{\tau} \quad (17)$$

From equations (15) and (17), the following mass and momentum equations are obtained:

$$\frac{\partial \rho}{\partial t} + \nabla \cdot \rho \vec{v} = 0 \quad (18)$$

$$\frac{\partial \rho \vec{v}}{\partial t} + \nabla \cdot \Pi = 0 \quad (19)$$

which are accurate to second order in ε for equation (2).

The momentum flux tensor Π has the form:

$$\Pi_{\alpha\beta} = \sum_i (\vec{e}_i)_\alpha (\vec{e}_i)_\beta \left[f_i^{eq} + \left(1 - \frac{1}{2\tau}\right) f_i^{(1)} \right], \quad (20)$$

and $(\vec{e}_i)_\alpha$ is the component of the velocity vector $\vec{e}_i$ in the α direction.

To specify the detailed form of $\Pi_{\alpha\beta}$, the lattice structure and the corresponding equilibrium distribution have to be specified. For simplicity and without loss of generality, the two-dimensional square lattice with nine velocities is considered,

$\vec{e}_i = (\cos(\pi(i-1)/4), \sin(\pi(i-1)/4))$ for i=1,3,5,7, (21)

$\vec{e}_i = \sqrt{2}(\cos(\pi(i-2)/4 + \pi/4), \sin(\pi(i-2)/4 + \pi/4))$ for i=2,4,6,8 , and

$\vec{e}_0 = 0$

Note that the NS equations have second-order nonlinearity. The general form of the equilibrium distribution function can be written up to $O(v^2)$ (Chen et al 1992):

$$f_i^{eq} = \rho\left[a + b\vec{e}_i \cdot \vec{v} + c(\vec{e}_i \cdot \vec{v}) + dv^2\right] \tag{22}$$

where *a*, *b*, *c*, and *d*, are lattice constants. This expansion is valid only for small velocities, or small Mach number v/c_s, where c_s is the *pseudo-sound-speed*. Using the constraints in equation (7), the coefficients in equation (22) can be obtained analytically (Qian et al 1992):

$$f_i^{eq} = \rho\, w_i\left[1 + 3\vec{e}_i.\vec{v} + \frac{9}{2}(\vec{e}_i.\vec{v})^2 - \frac{3}{2}v^2\right] \tag{23}$$

with

$$\begin{aligned} w_0 &= \frac{4}{9} \\ w_i &= \frac{1}{9} \quad i = 1,3,5,7 \\ w_i &= \frac{1}{36} \quad i = 2,4,6,8 \end{aligned} \tag{24}$$

Inserting the above formula into equation (20),

$$\begin{aligned} \Pi_{\alpha\beta}^{(0)} &= \sum_i (\vec{e}_i)_\alpha (\vec{e}_i)_\beta f_i^{eq} = p\delta_{\alpha\beta} + \rho \vec{v}_\alpha \vec{v}_\beta \\ \Pi_{\alpha\beta}^{(1)} &= \left(1 - \frac{1}{2\tau}\right)\sum_i (\vec{e}_i)_\alpha (\vec{e}_i)_\beta f_i^1 = \nu\left(\nabla_\alpha(\rho\vec{v}_\beta) + \nabla_\beta(\rho\vec{v}_\alpha)\right) \end{aligned} \tag{25}$$

where $p = \rho c_s^2 = \rho/3$ is the pressure, and $\nu = \left(\tau - \frac{1}{2}\right)c_s^2$ is the kinematic viscosity.

The resulting momentum equation is

$$\rho\left(\frac{\partial\vec{v}}{\partial t} + \nabla_\beta \cdot \vec{v}_\alpha \vec{v}_\beta\right) = -\nabla_\alpha p + \nu\nabla_\beta \cdot \left(\nabla_\alpha \rho\vec{v}_\beta + \nabla_\beta \rho\vec{v}_\alpha\right) \tag{26}$$

which is exactly the same as the Navier-Stokes equations for small density variation $\delta\rho$. Density variations in the LBM control pressure variations, which decide the magnitude of velocity; therefore, small density variations restriction can easily be translated into low Reynolds number restriction. The equation (26) represents the NS equations if *Re* is O(1). Figure 1 illustrates the two basic steps of the LBM.

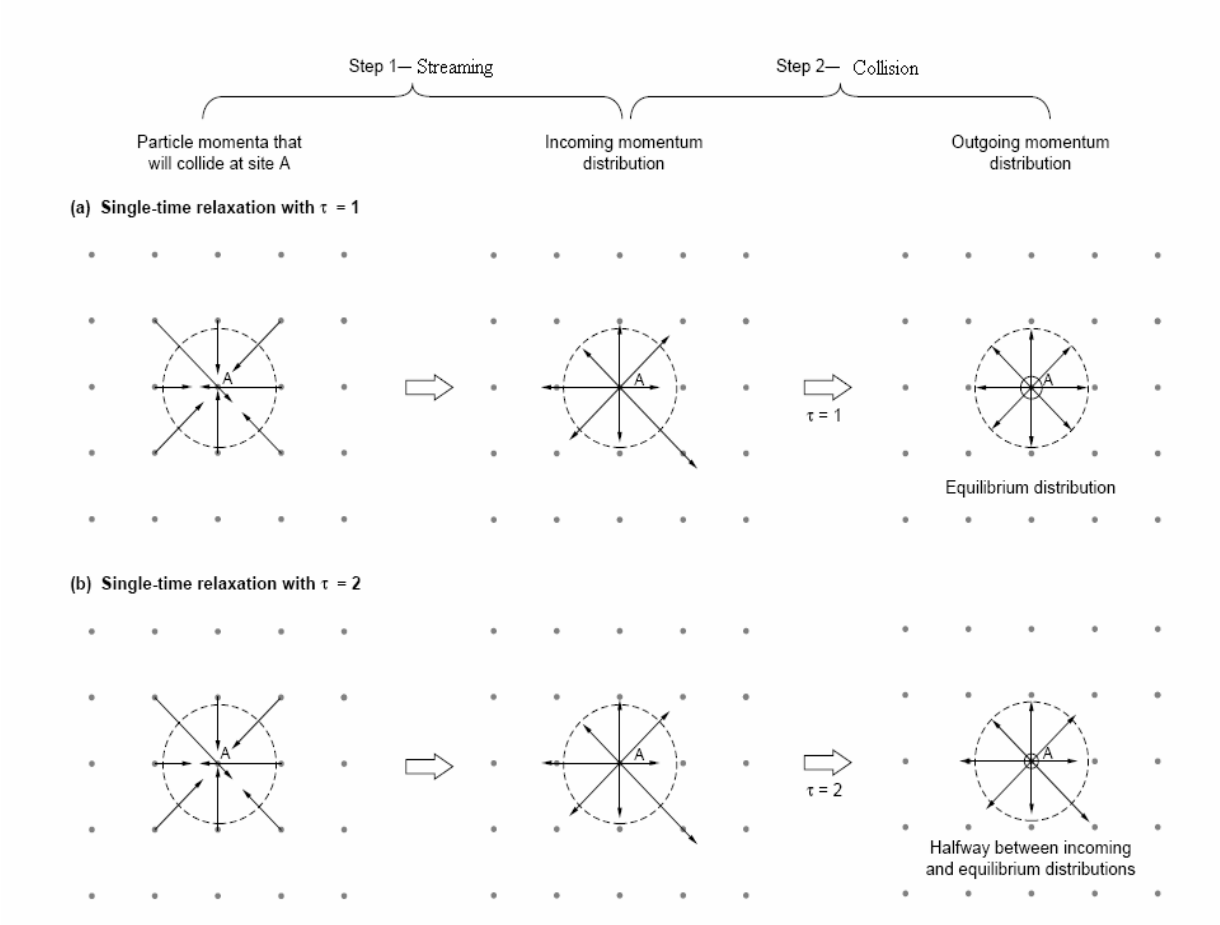

Figure 1: Basic steps in the LBM

Boundary Conditions

The wall boundary conditions in the LBM were originally taken from the LG method. For example, a particle distribution function bounce-back scheme (Wolfram 1986, Lavallee et al 1991) was used at walls to obtain no-slip velocity conditions. By the so-called bounce-back scheme, it is understood that when a particle distribution streams to a wall node, the particle distribution scatters back to the node it came from. The easy implementation of this no-slip boundary condition by the bounce-back boundary scheme supports the idea that the LBM is ideal for simulating fluid flows in complicated geometries, such as flow through porous media. Figure 2 shows the bounce-back boundary condition.

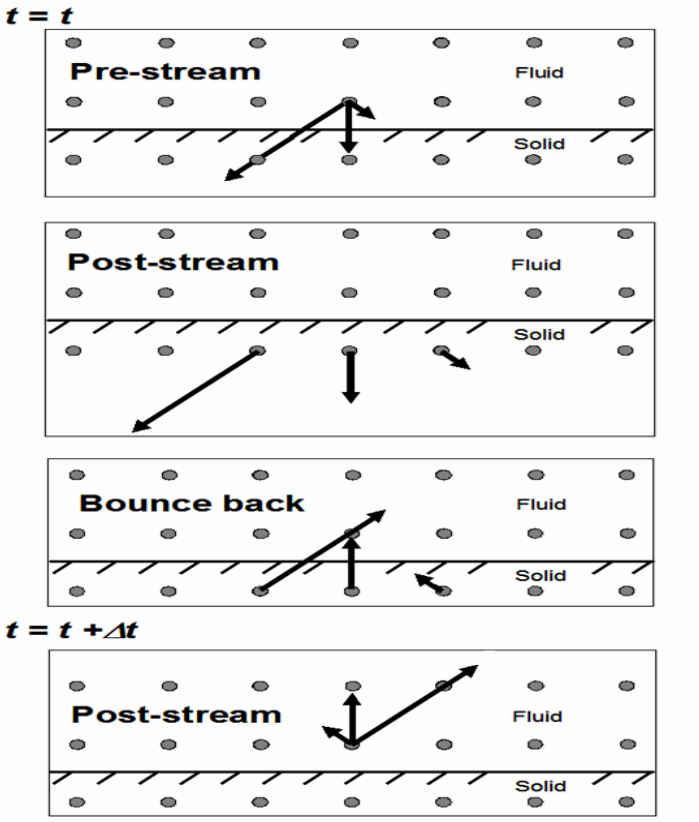

Figure 2: No-slip boundary condition

For a node near a boundary, some of its neighboring nodes lie outside the flow domain. Therefore the distribution functions at these no-slip nodes are not uniquely defined. The bounce-back scheme is a simple way to fix these unknown distributions on the wall node. On the other hand, it was found that the bounce-back condition is only first-order in numerical accuracy at the boundaries. This degrades the accuracy of the LBM, because the numerical accuracy of the LBM in equation (2) for the interior mesh is second-order.

To improve the numerical accuracy of the LBM, other boundary treatments have been proposed. Skordos (1993) suggested including velocity gradients in the equilibrium distributions at the wall nodes. Noble et al. (1995) proposed using hydrodynamic boundary conditions on no-slip walls by enforcing a pressure constraint. Inamuro et al (1995) recognized that a slip velocity near wall nodes could be induced by the bounce-back scheme and proposed to use a counter slip velocity to cancel that effect.

Application of LBM

Modeling of incompressible fluids. Due to severe limitations on time-step and grid-size, the LBM is practically limited to the modeling of incompressible and low- Reynolds number flows.

Modeling of thermal flows. Modeling of the complete set of transport equations using the discrete kinetic approach involves significant difficulties. There are three major problems in LBGK thermodynamics. First, the thermal LBGK models are limited to Pr=1/2 due to a single relaxation time (Alexander et al, 1993). Second, the thermal LBGK models have severe limitations on allowable variations of temperature and velocity due to the limited

set of the discrete particle velocities. Third, the 'thermal' LGBK models are prone to numerical instabilities due to the very large number of discrete velocities required to recover correct macroscopic equations (Huang et al. 1997; Boghosian and Coveney 1998; McNamara et al. 1995; Sun 2000; McNamara et al. 1997). For these reasons, the thermal LBGK models are found to be inferior to 'continuum CFD' finite-difference methods.

Modeling of thermodynamic behavior. Several LB methods were developed to account for 'non-ideality,' external forcing, and different phenomena associated with intermolecular interactions. Extension of the LB methods to non-uniform gases, and more generally to fluid-fluid multiphase flows, is accomplished either heuristically (by applying certain rules which mimic complex-fluid behavior); or based on Enskog's extension of the Boltzmann's theory of dense gases, with incorporation of the phenomenological models of quasi-local equilibrium constant temperature thermodynamics; and using the LB methodology to couple the latter one to the hydrodynamics of complex fluid. The major challenge is to accurately describe the physical mechanisms that govern the interface evolution (transport, breakup, and coalescence). Considering interfaces, one naturally and intuitively thinks in terms of molecules of different kinds, interacting over very short distances across the interfaces. Thus, intuitively, the models operating with the concept of particles and molecules should have methodological advantages over the methods of the 'continuum mechanics.'

Modeling of particulate suspensions in incompressible fluids. The LBM has been successfully applied to particulate suspensions in incompressible fluids, a class of

problems with complex geometries and moving boundaries. The key here is to accurately account for the momentum transfer across the solid-fluid boundary while conserving mass (Aidun and Lu, 1995; Aidun et al, 1998).

Chapter 2

Literature Review

Multiphase Lattice Boltzmann Method

Simulation of multiphase and multicomponent flows is important in many engineering applications, including flow through porous media, coating flow, boiling dynamics, and dendrite formation. There are several popular Lattice Boltzmann (LB) techniques for the analysis of multiphase flows, three of which are the methods of Gunstensen et al (1991), Shan & Chen (1993, 1994), and free energy approach by Swift et al. (1995, 1996). All three methods have been studied extensively with their distinct advantages (see review article by Nourgaliev et al, 2003). Out of the three, the method of Gunstensen (1991) is the oldest and simplest technique which can prescribe the interfacial dynamics by preferentially redistributing the single-particle probability functions in the direction of the normal color gradient.

Rothman & Keller (1988) were the first to extend the single-phase lattice gas (LG) model proposed by Frisch, Haslacher, and Pomeau (1986) to simulate multiphase fluid problems. Colored particles were introduced to distinguish between phases, and a nearest-neighbor particle interaction was used to facilitate interfacial dynamics, such as Laplace's formula for surface tension. Later, Somers and Rem (1991), and Chen et al. (1991) extended the original colored particle scheme by introducing colored holes. It has been shown that the colored-hole lattice gas method extends the original nearest-neighbor particle interaction to several lattice lengths, leading to Yukawa potential of the form $e^{-\lambda r}$ / r where λ is a physical constant and r is the radius vector.

The method of Gunstensen (1991) is based on the two-component LG model proposed by Rothman & Keller (1988). Later, Grunau et al. (1993) extended this model to allow variations of density and viscosity. In these models, red and blue particle distribution functions $f_i^{(r)}(\vec{x},t)$ and $f_i^{(b)}(\vec{x},t)$ are introduced to represent two different fluids. The effect of surface tension is obtained by adding another collision operator to the original BGK collision operator. The new operator redistributes the particle density functions in the direction normal to the color gradient. The additional collision step does not cause the phases to separate. To maintain interfaces or to separate the different phases, the LBM by Gunstensen et al. follows the LG method of Rothman & Keller to force the local color momentum to align with the direction of the local color gradient after collision. This step forces the fluids to move toward the same color. This method is very simple and powerful though it can be improved in some aspects. The prescribed surface tension is not explicit, meaning that the parameters used in the method do not give a direct control over the surface tension values. The perturbation step with the redistribution of colored distribution functions causes an anisotropic surface tension that induces unphysical vortices near the interfaces. The method does not account for dynamic normal stress applicable to a moving interface.

Method of Gunstensen et al.

Gunstensen et al. (1991) were the first to develop the multicomponent LBM method based on the two-component LG model proposed by Rothman & Keller (1988). Later, Grunau et al. (1993) extended this model to allow variations of density and viscosity. In

these models, red and blue particle distribution functions $f_i^{(r)}(\vec{x},t)$ and $f_i^{(b)}(\vec{x},t)$ are introduced to represent two different fluids. The total particle distribution function (or the color-blind particle distribution function) is defined as: $f_i = f_i^{(r)} + f_i^{(b)}$. The LBM equation is written for each phase:

$$f_i^k(\vec{x}+\vec{e}_i, t+1) = f_i^k(\vec{x}, t) + \Omega_i^k(\vec{x}, t) \tag{27}$$

where *k* denotes either the red or blue fluid, and

$$\Omega_i^k = \left(\Omega_i^k\right)^1 + \left(\Omega_i^k\right)^2 \tag{28}$$

is the collision operator. The first term in the collision operator, $\left(\Omega_i^k\right)^1$, represents the process of relaxation to the local equilibrium.

$$\left(\Omega_i^k\right)^1 = \frac{-1}{\tau}\left(f_i^k - f_i^{eq,k}\right) \tag{29}$$

Here, $f_i^{eq,k}$ is the local equilibrium distribution depending on the local macroscopic variables ρ_k and $\vec{v}$. τ_k is the characteristic relaxation time for species *k*. The viscosity of each fluid can be selected by choosing the desired τ_k. Conservation of mass for each phase and total momentum conservation are enforced at each node during the collision process:

$$\begin{aligned}
\rho_r &= \sum_i f_i^r = \sum_i f_i^{eq,r} \\
\rho_b &= \sum_i f_i^b = \sum_i f_i^{eq,b} \\
\rho\vec{v} &= \sum_{i,k} f_i^k \vec{e}_i = \sum_{i,k} f_i^{eq,k} \vec{e}_i
\end{aligned} \tag{30}$$

where $\rho = \rho_r + \rho_b$ is the total density and $\rho\,\vec{v}$ is the local total momentum. The form of $f_i^{eq,k}$ can be chosen to be similar to:

$$f_i^{eq,k} = \rho_k w_i \left[1 + 3\vec{e}_i.\vec{v} + \frac{9}{2}(\vec{e}_i.\vec{v})^2 - \frac{3}{2}\vec{v}^2 \right] \quad (31)$$

The additional collision operator $(\Omega_i^k)^2$ contributes to the dynamics in the interfaces and generates a surface tension:

$$(\Omega_i^k)^2 = \frac{A_k}{2}|F|\left(\frac{(e_i.F_i)^2}{|F|^2} - \frac{1}{2} \right) \quad (32)$$

where $\vec{F}$ is the local color gradient, defined as:

$$\vec{F}(\vec{x}) = \sum_i \vec{e}_i(\rho_r(\vec{x}+\vec{e}_i) - \rho_b(\vec{x}+\vec{e}_i)) \quad (33)$$

Note that in a single-phase region of the incompressible fluid model, $\vec{F}$ vanishes. Therefore, the second term of the collision operator only contributes to the interfaces and mixing regions. The parameter A_k is a free parameter, which determines the surface tension. The additional collision term does not cause the phase segregation. To maintain interfaces or to separate the different phases, the LBM by Gunstensen et al. follows the LG method of Rothman & Keller (1988) to force the local color momentum, $\vec{j} = \sum_i (f_i^r - f_i^b)\vec{e}_i$, to align with the direction of the local color gradient after collision. In other words, the colored distribution functions at interfaces are redistributed to maximize $-\vec{j} \circ \vec{F}$. Intuitively, this step will force colored fluids to move toward fluids with the same colors.

Method of Shan & Chen

Shan & Chen (1993) used microscopic interactions to modify the surface-tension-related collision operator for which the surface interface can be maintained automatically. In these models, $\left(\Omega_i^k\right)^2$ in equation (32) was replaced by the following expression:

$$\left(\Omega_i^k\right)^2 = \vec{\mathrm{e}}_i.\vec{\mathrm{F}}^k \tag{34}$$

$$\text{where } \vec{\mathrm{F}}^k = -\sum_{k'}\sum_i V_{kk'}(\vec{\mathrm{x}}, \vec{\mathrm{x}} + \vec{\mathrm{e}}_i)\,\vec{\mathrm{e}}_i \tag{35}$$

Here $V_{kk'}$ is an interaction pseudopotential between different phases:

$$V_{kk'} = G_{kk'}(\vec{\mathrm{x}}, \vec{\mathrm{x}}')\,\psi^k(\vec{\mathrm{x}})\psi^{k'}(\vec{\mathrm{x}}') \tag{36}$$

$G_{kk'}(\vec{\mathrm{x}})$ is the strength of the interaction; and $\psi^k(\vec{\mathrm{x}})$ is a function of density for the *k* phase at $\vec{\mathrm{x}}$ with the following empirical form : $\psi = \rho_0\left[1 - \exp\left(\frac{-\rho}{\rho_0}\right)\right]$, where ρ_0 is a constant, free parameter. It was shown that this form of the effective density ψ gives a non-ideal equation of state, which separates phases.

Free Energy Approach

The above multiphase and multicomponent lattice Boltzmann models are based on phenomenological models of interface dynamics and are probably most suitable for isothermal multicomponent flows. One important improvement in models using the free-energy approach (Swift et al. 1995, 1996) is that the equilibrium distribution can be defined consistently based on thermodynamics. Consequently, the conservation of the total energy, including the surface energy, kinetic energy, and internal energy can be properly satisfied.

The van der Waals formulation of quasilocal thermodynamics for a two-component fluid in thermodynamics equilibrium at a fixed temperature has the following free-energy functional:

$$\Psi(\vec{\mathrm{x}}) = \int d\vec{\mathrm{x}}\left[\psi(T,\rho) + W(\nabla\rho)\right] \tag{37}$$

The first term in the integral is the bulk free-energy density, which depends on the equation of state. The second term is the free-energy contribution from density gradients and is related to the surface tension. For simple multiphase fluid, flows, $W = \frac{\kappa}{2}(\nabla\rho)^2$, where κ is related to the surface tension.

Present Method

The method discussed in the present study aims at resolving the interface precisely using the Volume-of-Fluid (VOF) concept in background of the Gunstensen's method. The basic ideas of Gunstensen's method are used, but with some fundamental improvements. Surface tension, which is implicitly provided in the Gunstensen's method, is explicitly supplied in the present method. The present method also takes normal stress into account to describe the interfacial dynamics. Spurious velocity, which is one of the shortcomings of the Gunstensen's method, is greatly reduced in the present method by delineating the dependence of surface tension on other physical parameters as viscosity and density. This new method can therefore handle considerably high density and viscosity ratios for incompressible flows.

Literature Review Summary

Multiphase Lattice Boltzmann has been established as a powerful tool for simulating complex flows. The local nature of the interfacial and particle dynamics makes the method a suitable candidate for parallel programming. The convective step (the streaming step) is already linear, so along with the parallelization characteristic of the LBM, it helps in reducing the computational time. The interfacial dynamics in the multiphase LBM is obtained either by using the non-ideal equation of state for the pressure or by adding an interaction potential between a pair of fluids. The method of Gunstensen does not use either of these two approaches, using instead an empirical method to simulate the surface tension at the interface. The method of Shan and Chen and the free energy method realize the importance of a non-equilibrium pressure tensor and consistently provide a way of simulating the surface tension. The method of Gunstensen, on the other hand, has a few advantages over the other two methods which are primarily based on the thermodynamical equations, by simplifying the process of application of the surface tension. However all three methods give an empirical equation for the surface tension parameter as a function of other physical parameters.

The present method understands the importance of a non-equilibrium pressure tensor, and simply modifies the pressure equation to account for the pressure and density jumps. The modified pressure equation is based on the non-ideal equation of state, which is justified by the presence of the surface tension. The present method also supports an explicit, theoretical equation for the surface tension parameter.

The recoloring step, which helps in segregating the two fluids, is an indispensable step in the multiphase LBM. The method of Gunstensen prescribes it with three constraints. The present method, also, uses the recoloring step with the same constraints. Because of the advantage of using VOF, the interface obtained is just two lattice cells wide, regardless of the density ratio.

The method of Shan and Chen and the free energy method have some limitation on the density and viscosity ratios. The present method tries to resolve this issue. But, due to the intrinsic limitations in the method of Gunstensen and the LBM, in general, these issues are not completely resolved.

Chapter 3

Present Numerical Scheme

The method presented in the present study is based on using the VOF approach to resolve the interface and interfacial cells. For the sake of argument, the method is used to solve two-phase flow using D2Q9 (2 dimensions, 9 velocity states) LBM. The VOF function is defined as

$$[\text{VOF}] = \frac{\rho_\alpha - \rho_\beta}{\rho_\alpha + \rho_\beta} \quad , \tag{38}$$

where the subscripts α and β denote the heavier and lighter fluids, respectively ρ and is the fluid density, which is a function of space.

The presented equations are non-dimensionalized by the *lattice velocity*

$$c = \frac{\Delta x}{\Delta t} \ , \ \Delta x = \Delta t = c = 1$$

The Lattice Boltzmann equation for both the α and β fluids can be written as:

$$f_i^k(\vec{x} + \vec{e}_i, t+1) = f_i^k(\vec{x}, t) + \Omega_i(\vec{x}, t) \quad , \ k = \alpha \text{ or} \beta \tag{39}$$

where $f_i^\alpha(\vec{x},t)$ and $f_i^\beta(\vec{x},t)$ are the single-particle distribution functions at position $\vec{x}$ and time t for the α and β fluids, respectively. Here i=0,1,….,8 is the link number on a 2D lattice, and k denotes either the α or β fluid. The collision operator,

$$\Omega_i = \frac{-1}{\tau_k}(f_i^k - f_i^{eq,k}) \tag{40}$$

represents the process of relaxation to the local equilibrium. Here, $f_i^{eq,k}$ is the local equilibrium state which depends on the local density and velocity, and τ_k is the *lattice relaxation parameter* for species *k*.

The equilibrium distribution functions are chosen with the following constraints:

$$\rho_\alpha = \sum_i f_i^\alpha = \sum_i f_i^{eq,\alpha} \tag{41}$$

$$\rho_\beta = \sum_i f_i^\beta = \sum_i f_i^{eq,\beta} \tag{42}$$

$$(\rho_\alpha + \rho_\beta)\,\vec{v} = \sum_i (f_i^\alpha + f_i^\beta)\vec{e}_i \tag{43}$$

For each fluid, the equilibrium distribution functions given by

$$f_i^{eq,\beta} = \rho_\beta w_i \left[1 + 3\vec{e}_i.\vec{v} + \frac{9}{2}(\vec{e}_i.\vec{v})^2 - \frac{3}{2}v^2 \right] \tag{44}$$

$$f_i^{eq,\alpha} = \rho_\alpha w_i \left[r_i + 3\vec{e}_i.\vec{v} + \frac{9}{2}(\vec{e}_i.\vec{v})^2 - \frac{3}{2}v^2 \right] \tag{45}$$

are used to ensure a thin interface. Here, $\vec{v}$ is the velocity vector, $\vec{e}_i$ is the *lattice velocity* of the ith link (For background and derivations of these relations, see Appendix A).

For the D2Q9 lattice:

$$\vec{e}_i = (\cos(\pi(i-1)/4), \sin(\pi(i-1)/4)) \quad \text{for} \quad i=1,3,5,7, \tag{46}$$

$\vec{e}_i = \sqrt{2}(\cos(\pi(i-2)/4 + \pi/4), \sin(\pi(i-2)/4 + \pi/4))$ for i=2,4,6,8 , and

$\vec{e}_0 = 0$

and

$$r_0 = 0.25\ (9 - \frac{5}{r})$$
$$r_i = \frac{1}{r}, \quad i = 1,...,8 \tag{47}$$

where $r = \frac{\rho_\alpha}{\rho_\beta}$, is the density ratio,

and

$$w_0 = \frac{4}{9}$$
$$w_i = \frac{1}{9} \quad i = 1,3,5,7$$
$$w_i = \frac{1}{36} \quad i = 2,4,6,8 \tag{48}$$

The body force and pressure gradient terms are added as:

$g_i = 3 w_i \vec{e}_i . \vec{g}$ where $\vec{g}$ = body force vector (49)

The method of Gunstensen suggests using another collision operator to apply surface tension effects at the interface. The present method skips this step, and instead suggests a new method to explicitly apply the surface tension. In the new method, surface tension is seen as the result of a body force acting normal to the interface in the interfacial region. The body force is proportional to the surface tension value, which satisfies the Laplace equation. Intuitively, the application of a body force leads to forcing the particle distribution functions normal to the interface. The extent of this forcing depends upon the local value of the radius of curvature of the interface.

Apart from accounting for the static stress jump, the new method attempts at including dynamic normal stress jump at the interface. The pressure jump [p] at a dynamic interface is given by,

$[p] = \sigma K + 2 [\mu (\nabla v_1 . \vec{n}, \nabla v_2 . \vec{n}) . \vec{n}]$, (50)

(for derivation of the above relation, see Appendix C),where $\vec{n}$ is the local unit normal vector to the interface, σ is the coefficient of surface tension, *K* is the local curvature of the interface, and μ is the fluid viscosity:

$$\vec{n} = \frac{\nabla[\mathrm{VOF}]}{|\nabla[\mathrm{VOF}]|} \tag{51}$$

$$K = n_1 n_2 (\partial_1 n_2 + \partial_2 n_1) - {n_2}^2 \partial_1 n_1 - {n_1}^2 \partial_2 n_2 \tag{52}$$

The viscosity of the two fluids:

$$\mu_k = \rho_k \left[\tau_k - \frac{1}{2} \right] c_{s,k}^2 \, \Delta t \tag{53}$$

where c_s is the *pseudo-sound-speed*, and $k = \alpha$ or β .Using the pressure jump relation of equation (50), the extra body force term can be written as:

$$g_i = 3 w_i \vec{e}_i . ((\sigma K + S_1) n_1, (\sigma K + S_2) n_2) \tag{54}$$

where

$(S_1, S_2) = 2 \left[\mu (\nabla v_1 . \vec{n}, \nabla v_2 . \vec{n}) \right]$ is the normal stress jump. (55)

Like the method of Gunstensen, a segregation step is used to ensure separation of the two phases. The method is based on the following three requirements: (1) Conservation of total mass (sum of α and β fluids), (2) Conservation of α and β masses, and (3) Conservation of total momentum.

The segregation step in the present method is preceded by a mixing step, which is invoked right before the collision step and after the streaming step. In an interfacial cell, the two fluids exist at the same location because of streaming. Coexistence of the two fluids requires two different collision operators, which may lead to two different velocity

vectors. Since there cannot be two different velocity vectors at one lattice point, the distribution functions are updated based on the magnitude of the VOF as follows:

- If $0<VOF_{\text{before mixing}}<1$ then $VOF_{\text{after mixing}}=1$;
- If $-1<VOF_{\text{before mixing}}<0$ then $VOF_{\text{after mixing}}=-1$.

The collision operator of the dominant fluid is used after converting the less-dominant fluid into the more-dominant fluid. After collision and application of the surface tension, the segregation step is invoked. The segregation step gives back the previously transferred distribution functions of the less dominant fluid, per the rules discussed before.

The interface obtained in the present method is two lattice cells wide; one with $[\text{VOF}] \geq 0$, and the other with $[\text{VOF}] < 0$; and it is obtained by searching for cells with at least one nearest neighbor with opposite sign of $[\text{VOF}]$.

Chapter 4

Numerical Simulations and Discussion

Several test problems were used to validate the proposed approach. The Laplace bubble test is used to examine how accurately the imposed value of surface tension relates to the physical surface tension. The two dynamic interfacial stability test problems, namely the Saffman-Taylor and Rayleigh-Taylor instabilities, are simulated to show the method's capability to accurately predict the interfacial dynamics. Finally, the method is applied to a dispersion of deformable viscous drops in a liquid. The results obtained are compared with those of Pozrikidis (1993) using the boundary element method.

The Laplace test is also used for estimating spurious velocity inside and around the bubble. One of the major drawbacks of the method of Gunstensen is its large value of spurious velocities which makes the code unstable for slightly higher values of Reynolds number. The method of Shan and Chen also suffers from large spurious velocities; however, its magnitude is greatly reduced. The free energy approach pronouncedly reduces this velocity and increases the stability of the code.

This method can simulate much higher viscosity ratios than other standard multiphase LB techniques. A maximum viscosity ratio of 30 was used in the Saffman-Taylor instability to produce a clear finger. A maximum density ratio of 5.5 was used in the Rayleigh-Taylor instability to illustrate the capabilities of this method for moderate density ratios.

Laplace Bubble Test

When a static spherical bubble of β fluid is immersed in the α fluid, the pressure jump Δp is given by Laplace's law,

$$\sigma = \Delta pR \tag{56}$$

or, $$\Delta p = \sigma K \tag{57}$$

Given the radius and the pressure jump from the simulation, one can compute the surface tension $\sigma_{Laplace}$ using equation (19) and compare it with the value provided to the present method. Then one can see if the applied value of surface tension causes a pressure jump commensurate to the Laplace relation. In all cases considered here, τ is taken as 1.0 for both fluids. A circular bubble is placed in the center of the control volume with a 501x501 grid. Pressure inside and outside of the bubble is calculated using the relation,

$$p = \rho_k \, c_{s,k}^2 \tag{58}$$

after 20,000 time steps (c_s is the *pseudo-sound-speed*, and $k = \alpha$ or β).

Table 1 Comparison between simulated and supplied values of surface tension

ρ_α	ρ_β	K	$\sigma_{\text{sup}\,plied}$	$\sigma_{simulated}$	Error Factor
0.99914	1.00639	0.1169	0.0200	0.0206	1.033
1.99854	1.01034	0.0180	0.2000	0.2050	1.025
2.97900	1.00931	0.1131	0.0500	0.0480	0.961
3.96980	1.00970	0.1150	0.0500	0.0500	1.000
4.99970	1.00610	0.0193	0.1000	0.1046	1.046
1.99773	1.00264	0.1237	0.0100	0.0101	1.017

In all cases the results are within ±5%. It is speculated that the error apparent in the table above is due to the inability to accurately calculate the curvature. At present, the

curvature is obtained as the average value of the curvature in the interfacial region. Therefore, even if the method gives the same value of surface tension as the supplied value the errors in calculating *K* introduce errors in the calculated surface tension value.

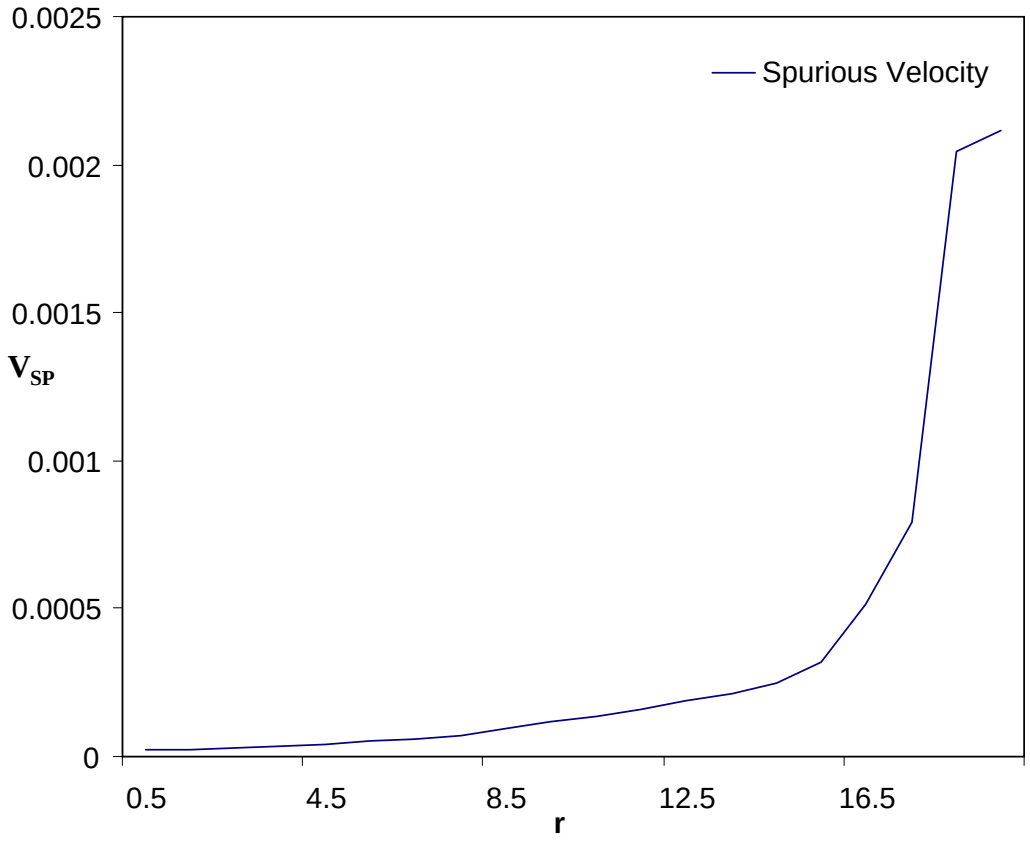

Figure 3: Variation of spurious velocity

Figure 3 shows the variation of spurious velocity inside and at the interface of a bubble of radius 20 lattice units. $\sigma = 0.01, \tau_\alpha = \tau_\beta = 1.0$, and $\rho_\alpha = \rho_\beta = 1.0$. The maximum spurious velocity which is of the order of 0.2% is found at the interface.

According to Nourgaliev et al. (2003), the method of Shan and Chen and the free-energy method have spurious velocity values of the order of 1% and 0.01%, respectively. The

present method is therefore somewhere in the middle of these two popular multiphase methods.

Saffman-Taylor Instability

If a less viscous fluid is driven into a more viscous one, the interface between the two fluids may become unstable, with long fingers of the less viscous fluid penetrating the bulk of the more viscous one. It was shown that the interface is unconditionally unstable in the absence of surface tension (Saffman & Taylor 1958), and that surface tension introduces a minimum wavelength for this instability.

Two dimensionless parameters can be used to determine this viscous fingering: the ratio of the kinematic viscosities between the displaced and displacing fluids ($M = \nu_2 / \nu_1$), and the other is the capillary number (Ca) defined as:

$$Ca = \frac{u_I \rho_2 \nu_2}{\sigma} \tag{59}$$

Here, u_I is the tip velocity of the interface, which is located at the center of the interface if no instability occurs and ρ_2 and ν_2 are density and viscosity of the displaced fluid. It is well known that the driving fluid forms a growing finger penetrating the displaced fluid instead of pushing it evenly if M and Ca are large enough. Figure 4 illustrates the schematic illustration of the simulation geometry, where W and T are the finger width and length, respectively, and S is the slip distance of the contact line.

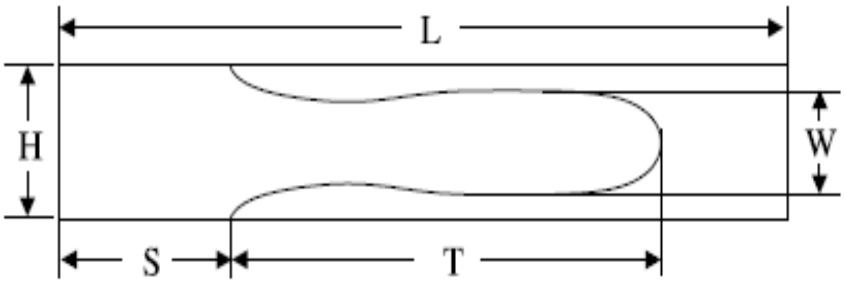

Figure 4: Schematic illustration of simulation geometry

In the simulation, the grid size is 321×41. No-slip boundary conditions are imposed on the top and bottom walls of figure 4. Initially, only bulk phase 2 (α fluid) is present in the channel. At zero time, the first two x-columns are set to contain only bulk phase 1 (β fluid). To avoid the boundary effects and to develop a steady finger, a Poiseuille velocity profile with maximum value u_0 is enforced at both the inlet and outlet.

Figures 5 (a-d) show the evolution of fingers for M=1, 10, 20, and 30, respectively. Figure 5(e) shows the case with high surface tension. The five contours in each figure correspond to VOF=0 at t = 0, 800, 1600, 2400, 3200 and 4000 time steps. τ_β is fixed at 0.6 . M=1, 10, 20, and 30 are obtained by choosing τ_α =0.6, 1.5, 2.5, and 3.5. In these simulations σ = 0.02 or 0.1, u_0 = 0.1 and $\rho_\alpha = \rho_\beta$.

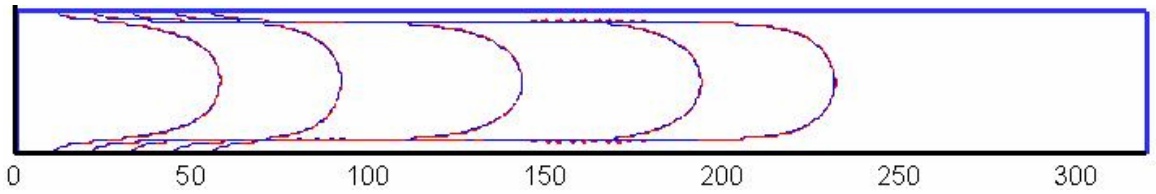

a), M = 1, σ = 0.02

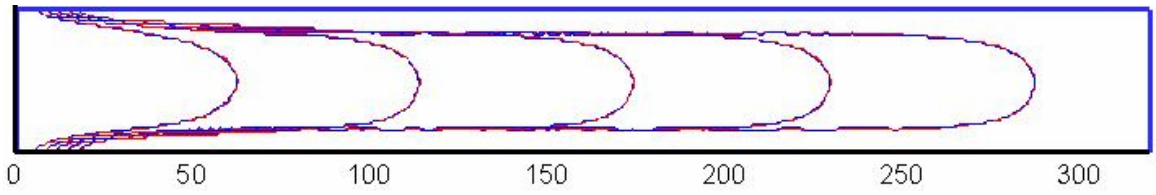

b), M = 10, σ = 0.02

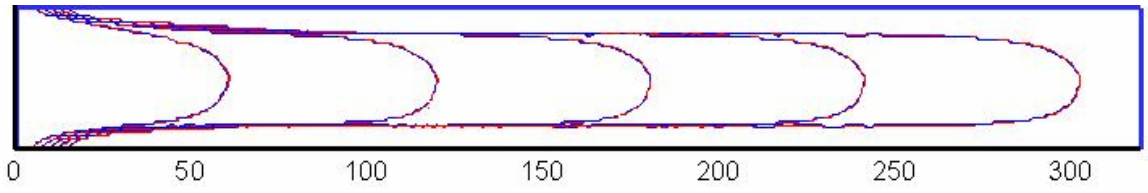

c), M = 20, σ = 0.02

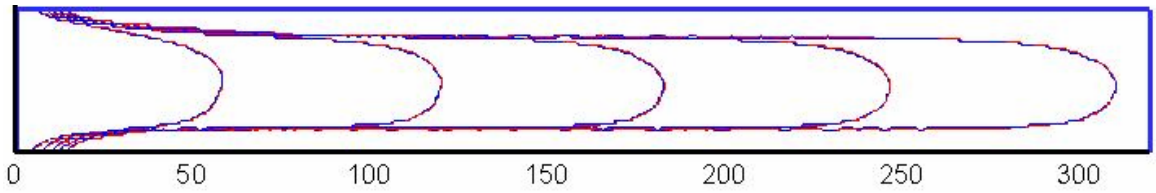

d), M = 30, σ = 0.02

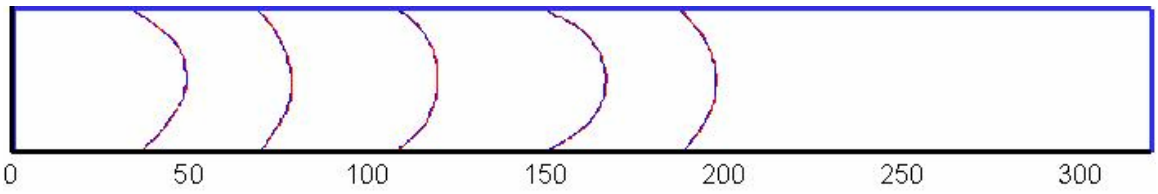

e), M = 1, σ = 0.1

Figure 5: Finger development in Saffman-Taylor instability

Table 2 Dimensionless finger width (W/H), finger length (T/L), and slip distance (S/L) of the contact lines at t = 4000 for different M for $u_0 = 0.1$

M	C_a	W/H	T/L	S/L
1	0.166	0.832	0.534	0.186
10	1.666	0.657	0.846	0.055
20	3.333	0.648	0.897	0.048
30	5.000	0.625	0.925	0.045

It can be seen from Table 2 that the finger width (W), length (T), and the slip distance (S) at time t = 4000 are different for different cases. Consistently, T increases but both W and S decrease as M increases. It has been established in literature (Saffman & Taylor 1958) that as M goes to infinity, W/H goes to 0.5. In our simulations, at the highest viscosity ratio of M=30, W/H = 0.62, which, in view of the decrease in W/H as M increases, suggests that these simulations may converge to this asymptotic value.

To compare the results obtained with the present method with the results of Kang, Zang, and Chen (2004), a different set of simulations were performed, where $\sigma = 0.02$, $u_0 = 0.1$ and $\rho_\alpha = \rho_\beta$, and the grid size was 400×66. Table 3 presents the comparison of the W/H values obtained by the present method and those obtained by Kang, Zang, Chen. The comparison shows that the two set of values match each other quite closely. Figure 6 plots the two set of values.

Table 3 Dimensionless finger width (W/H) at t = 5000 for different M for $u_0 = 0.1$

M	C_a	$(W/H)_{\text{present method}}$	$(W/H)_{\text{Kang ,Zang ,Chen}}$
1	0.697	0.751	0.743
4	0.722	0.710	0.706
10	0.754	0.678	0.673

The method doesn't take the wettability or the three-point contact line motion into account, which is considered by Kang, Zang, and Chen in their study. Therefore, the other physical parameters related to finger formation are not compared, as they are affected by the cohesive and adhesive forces existing between the liquids and the wall.

It is speculated that if a preferential interaction potential, leading to attractive forces for wetting fluids and repulsive forces for non-wetting fluids, is added, some of the features of the three-point contact line motion can be incorporated in the method.

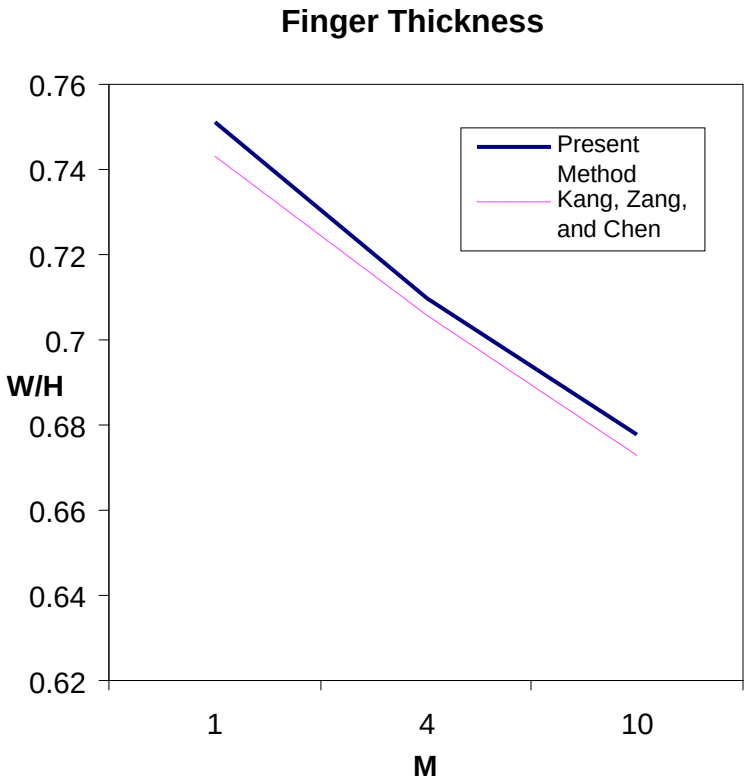

Figure 6: Comparison of finger thickness

The film thickness at the wall δ has been studied extensively and modeled by several empirical correlations, of which the best-known is that of Bretherton (1961):

$$\frac{2\delta}{D-2\delta} = 1.34Ca^{2/3} \tag{60}$$

where D is the tube diameter. Aussillous and Quere (2000) obtained a more accurate correlation using an empirical curve fit for different viscosity oils:

$$\frac{2\delta}{D} = \frac{1.34Ca^{2/3}}{1+2.5\times 1.34Ca^{2/3}} \tag{61}$$

If 'D' in the above correlation is replaced by 'H,' the channel height, then a comparison between the literature and simulated values of the film thickness can be performed.

$$\frac{2\delta}{H} + \frac{W}{H} = 1 \tag{62}$$

Table 4 Comparison of film thickness

M	C_a	$\frac{2\delta}{H}_{simulated}$	$\frac{2\delta}{H}_{Aussillous,Quere}$
10	1.666	0.343	0.323
20	3.333	0.352	0.353
30	5.000	0.375	0.363

The results show very good agreement between the two sets of the film thickness values.

Rayleigh-Taylor Instability

The Rayleigh-Taylor (RT) (1950) instability occurs when a low-density fluid is driven into a high-density fluid, or a heavy fluid lies above a light fluid in a gravitational field. In the case of heavy fluid lying above the light fluid, the interface is in an unstable equilibrium, if there is no disturbance at the interface. However, depending upon the wavelength of the disturbance, the interface can become unstable leading to heavy fluid moving downward and bubbles of light fluid moving upward.

The wavelength of the disturbance at which the interface is just stable is called the neutral wavelength. The system becomes unstable slightly above the neutral wavelength. For a 2D system, neutral wavelength (λ_n) is given by (Lamb 1945):

$$\lambda_n = 2\pi\sqrt{\frac{\sigma}{\Delta\rho g}} \tag{63}$$

where $\Delta\rho$ is the difference in densities and g is the gravitational acceleration.

In the present case, the values of neutral wavelength obtained in the simulation are compared with the theoretical values. In all cases, the ratio of surface tension to gravity is taken as constant, equal to 200. Periodic boundary condition is used to force the width of the channel as the wavelength of the disturbance.

Table 5 Comparison between theoretical and simulated values of neutral wavelength(λ_n)

$\Delta\rho / \rho_\beta$	$\lambda_n(Theoretical)$	$\lambda_n(Simulated)$	Error = difference
1.0	88.85	90.00	1.15
1.5	72.55	74.00	1.45
2.0	62.83	68.00	5.17
2.5	56.19	61.00	4.81
3.0	51.30	55.00	4.70
3.5	47.49	53.00	5.51
4.0	44.42	49.00	4.58
4.5	41.88	46.00	5.12

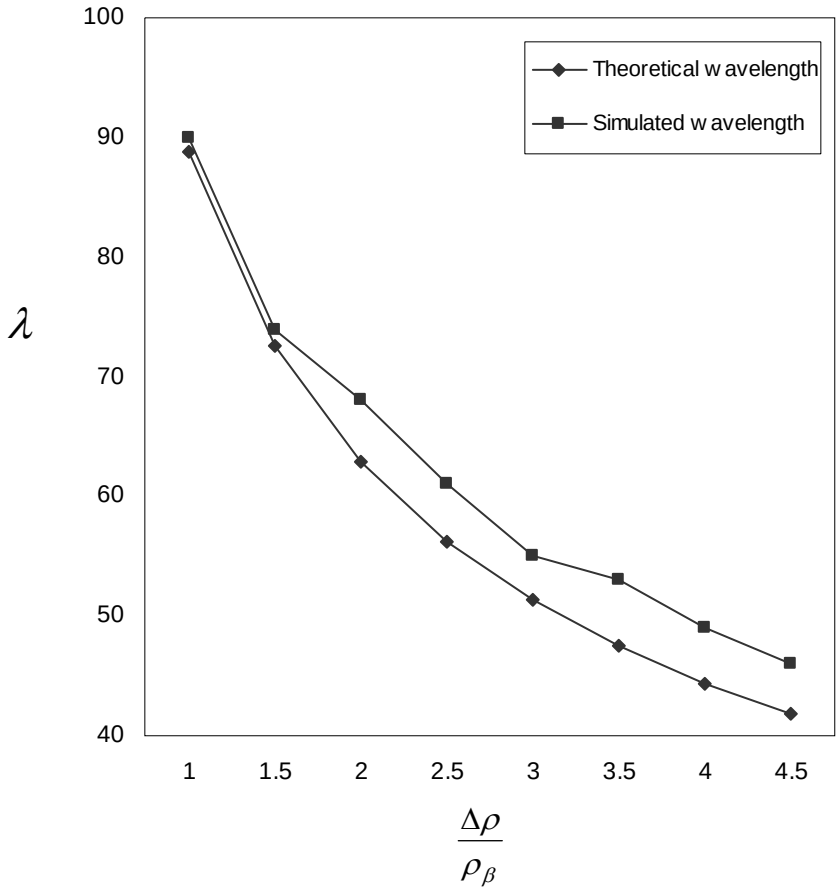

Figure 7: Comparison between simulated and theoretical values of neutral wavelength

The error shown in Figure 7 is conjectured to be due to three factors: (1) the growth rates of the disturbance at wavelengths marginally above the neutral wavelength are almost zero, resulting in overestimation of the neutral wavelength; (2) the inability of the method to correctly calculate the local values of the curvature, as the interface is two lattice cells wide; (3) the mesh size. The error, in almost all cases, is close to 4 units.

The importance of the mesh size in terms of this error was evaluated by carrying out another set of simulations with a refined global mesh. The ratio of the surface tension to gravity was taken to be 800 in order to obtain higher values of the theoretical neutral wavelength. This ratio of the surface tension to gravity gives a two-fold finer mesh. For the case of $\Delta\rho$ =2.0, g = -0.00005, σ =0.04, and $\tau_\alpha = \tau_\beta$ =0.8, the theoretical value of the neutral wavelength is 126 lattice units, and the simulated value is 131 lattice units;

therefore the percentage error is 3.9 %, which is more than half the error obtained with the coarse mesh. The error due to the factor (1) is conjectured to remain constant with increasing mesh resolution, but the error due to the factor (2) and (3), as seen in the simulation discussed above, decreases with increasing mesh resolution.

Flow of Drops Suspended in a Channel

The flow of suspensions of flexible particles, such as drops, cells, and capsules, in simple shear involves a variety of motions that lead to their deformation and breakup. In the present study, cylindrical drops in two-dimensional flow at low Reynolds number are used to understand the behavior of deformable suspensions in simple shear. The phenomenon of drop deformation and breakup has been studied extensively. The simplicity of two-dimensional flows was exploited by investigators such as Richardson (1968, 1973) who studied the behavior of two-dimensional solitary bubbles in a purely straining flow, a simple shearing flow, and a parabolic flow; Buckmaster (1973) and his co-workers, who studied the deformation and breakup of 2D slender drops with pointed ends in a purely straining flow; and Pozrikidis and Zhuo (1993) who studied the flow of a periodic suspension of two-dimensional viscous drops between two parallel plates.

In the context of two-dimensional flow, one configuration which has received attention on several occasions consists of a suspension of two-dimensional particles at low Reynolds number arranged in a single file within a channel that is bounded by two parallel plane walls. In the present study, the motion of a single file of initially circular drops between two parallel plates is being considered. The separation between two drops

is equal to the width of the channel, i.e., L=2H. The half-width of the channel H is used to non-dimensionalize all length scales. We find that the motion of the suspension depends on three parameters that include the viscosity ratio λ, the capillary number $\mu U / \sigma$, and the drop radius 'a.'

The results show that as Ca is increased, the drop obtains a more eccentric elliptic shape and, finally, a sigmoidal shape. There is a critical value of Ca, above which the drops do not reach a steady state and, instead, continue to deform and elongate under the action of the shearing flow generated by the motion of the two walls (figure 8). The deformation variable D = (L-M)/(L+M), where L and M are respectively the maximum and the minimum dimensions of the drop, respectively, vary almost linearly with Ca up to the critical value of Ca above which the drop does not attain a stable state.

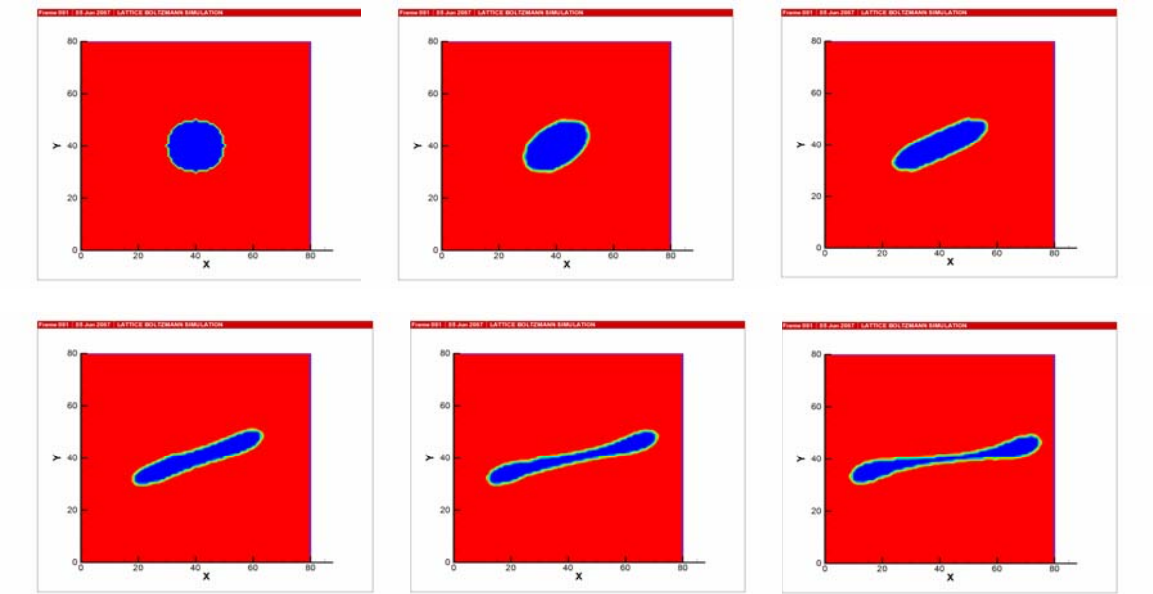

Figure 8: Evolution of bubble deformation at t=1000, 2000,3000,4000,5000, and 6000 timesteps

The orientation angle θ spans a range of values from $\pi/4$ to $\pi/20$. The critical value of Ca is around 3.5.

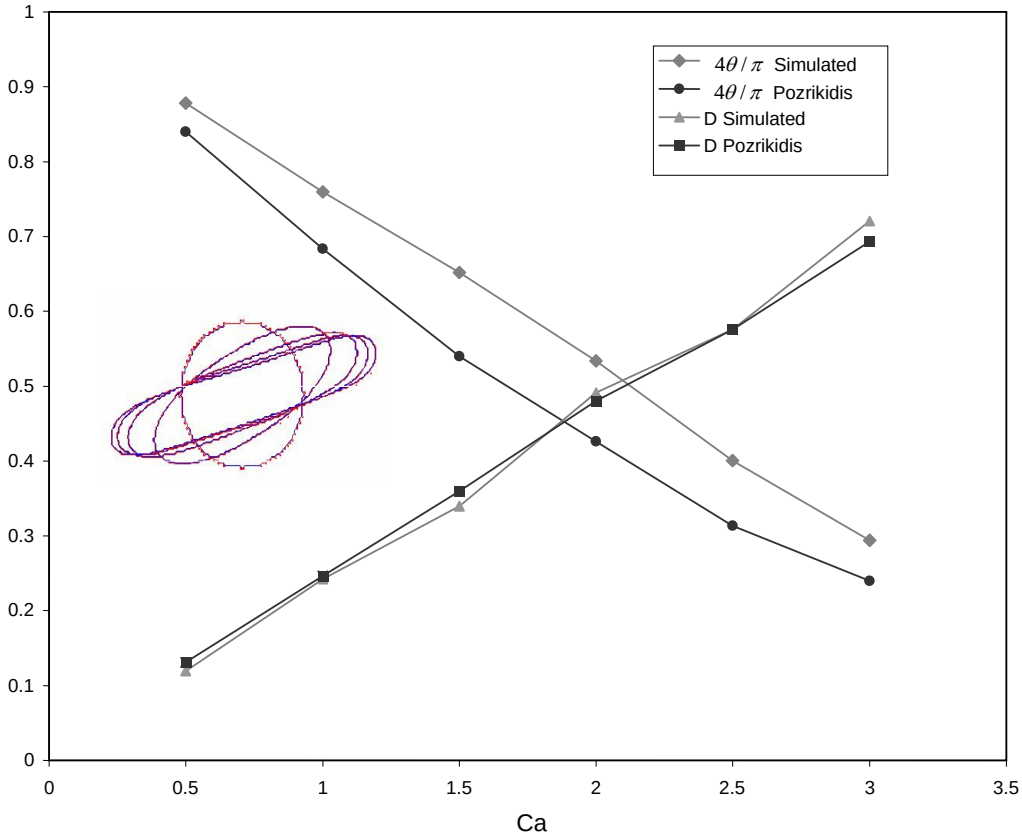

Figure 9: Variation of D and θ with Ca for λ=1 and a=0.25

The D values obtained in the simulation match quite closely with the D values obtained by Pozridikis (1993); however there is small mismatch between the θ values (Figure 9). The author is not sure about the reason of this mismatch, although it is likely that the mismatch would decrease with a finer mesh.

Chapter 5

Conclusion

In the present study, a Volume-of-Fluid based multiphase lattice Boltzmann method was aimed for development. The method of Gunstensen was taken as the base method on which certain improvements were imposed. Out of the several improvements, the most important are the explicit application of the surface tension and the inclusion of the normal stress jump at the interface. The method was developed with a thin interface and capability for high viscosity and density ratios as requirements. The method was tested against four test problems, and comparisons were made with other numerical, experimental, and theoretical works. After the successful simulation of the test problems, it can be concluded that the method successfully captures the physics involved in the multiphase systems.

In the Laplace test, the simulated values of the surface tension show good agreement with the input values. There is some mismatch between the two, which has been ascribed to the inability of the method to correctly evaluate the local curvature values. Spurious Velocity are found to be of the order of 0.2 %, which is somewhere in the middle of the spurious velocities for the two popular multiphase methods. More or less, the method shows good results for easy control of the surface tension values, as aimed by the present study.

In the Saffman-Taylor instability, a clear finger forms for a high capillary number and viscosity ratio. The normal stress at the interface comes into effect as the interface moves

forward. The capability to simulate for higher values of viscosity ratio is successfully demonstrated with consistent results. The finger formation is successfully compared with other works in the same field.

In the Rayleigh-Taylor instability, due to the inherent fluid flow, large velocity gradients and spurious velocity, for the high density ratio cases, make the code unstable. Therefore, normal stress component is relaxed for high density ratio cases, as we are only interested in the onset of the instability, not in the flow field. The method shows encouraging results for the Rayleigh-Taylor instability. The apparent error in the simulated values of neutral wavelengths can be attributed to the method's inability to exactly calculate the local values of curvature, and the fact that the instability growth rates are almost zero just above the neutral wavelength value.

In the simulation for drops in an ambient fluid, the method correctly estimates the shape of the drop. The results obtained can be compared quite closely with the results of Pozrikidis to show that the method is indeed capturing the correct physics.

Appendix A

Local Grid Refinement

In the present method, location of the interface is known at every time step with the precision of two lattice cells; therefore, local grid refinement can be done around the interface for better interfacial dynamics, especially for evaluation of physical parameters such as the normal vector and curvature.

Grid refinement in the present method is different from conventional grid refinement as the position of the interface changes after every time-step. Dynamic local grid refinement leads to formation of two more interfaces around the physical interface: the coarse-mesh interface and the fine-mesh interface, which move according to the movement of the physical interface.

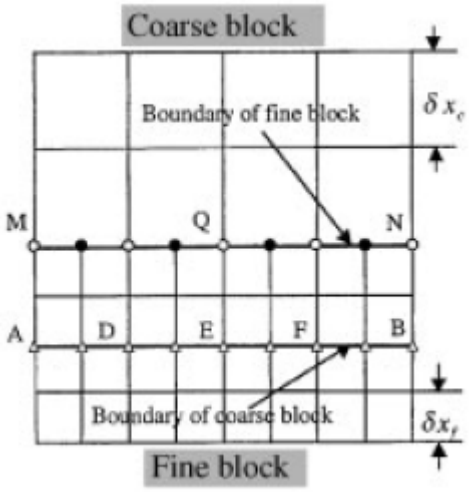

Figure 10: Fine block and coarse block boundaries

To illustrate the basic idea, a two-block system (a coarse and a fine grid) is considered in the derivation for the interfacial information exchange. The ratio of the lattice space between the two-grid system is

$$m = \frac{\Delta x_c}{\Delta x_f} \tag{64}$$

For a given lattice size Δx, the viscosity of the fluid is

$\nu_k = \left[\tau_k - \frac{1}{2}\right] \mathrm{c}_{s,k}^2 \, \mathrm{c} \, \Delta x$, $k = \alpha$ or β , where c is the *lattice speed.*

In order to keep a consistent viscosity, and thus *Re*, in the entire flow field involving different *lattice* sizes, the relation between relaxation times, $\tau_{f,k}$, on the fine grid, and, $\tau_{c,k}$, on the coarse grid, must obey the following rule:

$$\tau_{f,k} = \frac{1}{2} + m\left(\tau_{c,k} - \frac{1}{2}\right) \tag{65}$$

for c = 1.

To keep the variables and their derivatives continuous across an interface between two different grids, a consistent and accurate relationship for the probability density function in the neighboring grid blocks must be developed.

It is noted that,

$$f_i^k(\vec{\mathrm{x}}, t) = f_i^{eq,k}(\vec{\mathrm{x}}, t) + f_i^{neq,k}(\vec{\mathrm{x}}, t) \tag{66}$$

where $f_i^{neq,k}$ is the non-equilibrium part of the distribution function based on which the deviatoric stresses are evaluated. The collision step gives

$$\tilde{f}_i^k(\vec{\mathrm{x}}, t + \Delta t) = \left(1 - \frac{1}{\tau_k}\right) f_i^k(\vec{\mathrm{x}}, t) + \frac{1}{\tau_k} f_i^{eq,k}(\vec{\mathrm{x}}, t) \tag{67}$$

where $\tilde{f}_i^k$ is the pre-streaming distribution function.

Substituting equation (66) into equation (67) leads to

$$\tilde{f}_i^k(\vec{x},t+\Delta t)=\left(1-\frac{1}{\tau_k}\right)\left[f_i^{eq,k}(\vec{x},t)+f_i^{neq,k}(\vec{x},t)\right]+\frac{1}{\tau_k}f_i^{eq,k}(\vec{x},t) \tag{68}$$

$$=f_i^{eq,k}(\vec{x},t)+\frac{\tau_k-1}{\tau_k}f_i^{neq,k}(\vec{x},t) \tag{69}$$

Denoting the coarse-grid quantities with the superscript *c* and fine-grid quantities with the superscript *f*, the post-collision, or pre-streaming, step gives

$$\tilde{f}_i^{(c)k}=f_i^{(c)eq,k}+\frac{\tau_{c,k}-1}{\tau_{c,k}}f_i^{(c)neq,k} \tag{70}$$

Similarly,

$$\tilde{f}_i^{(f)k}=f_i^{(f)eq,k}+\frac{\tau_{f,k}-1}{\tau_{f,k}}f_i^{(f)neq,k} \tag{71}$$

Since the velocity and density must be continuous across the interface between the two grids

$$f_i^{(c)eq,k}=f_i^{(f)eq,k} \tag{72}$$

To maintain continuity in deviatoric stress, in the 2-D case,

$$\Pi_{\alpha\beta}=\left(1-\frac{1}{2\tau}\right)\sum_i f_i^{neq,k}(\vec{e}_{i\alpha}\cdot\vec{e}_{i\beta}-\frac{1}{2}\vec{e}_i\cdot\vec{e}_i\delta_{\alpha\beta}) \tag{73}$$

It is obvious that one requires

$$\left(1-\frac{1}{2\tau_{c,k}}\right)f_i^{(c)neq,k}=\left(1-\frac{1}{2\tau_{f,k}}\right)f_i^{(f)neq,k} \tag{74}$$

$$f_i^{(c)neq,k}=m\frac{\tau_{c,k}}{\tau_{f,k}}f_i^{(f)neq,k} \tag{75}$$

Substituting equation (75) into equation (70) one obtains

$$\tilde{f}_i^{(c)k} = f_i^{(c)eq,k} + m\frac{\tau_{c,k}-1}{\tau_{f,k}} f_i^{(f)neq,k} \tag{76}$$

Using equations (71) and (72), the above becomes

$$\tilde{f}_i^{(c)k} = f_i^{(f)eq,k} + m\frac{\tau_{c,k}-1}{\tau_{f,k}-1}\left[\tilde{f}_i^{(f)k} - f_i^{(f)eq,k}\right] \tag{77}$$

In transferring the data from the coarse grids to the fine grids, one similarly obtains

$$\tilde{f}_i^{(f)k} = f_i^{(c)eq,k} + \frac{\tau_{f,k}-1}{m(\tau_{c,k}-1)}\left[\tilde{f}_i^{(c)k} - f_i^{(c)eq,k}\right] \tag{78}$$

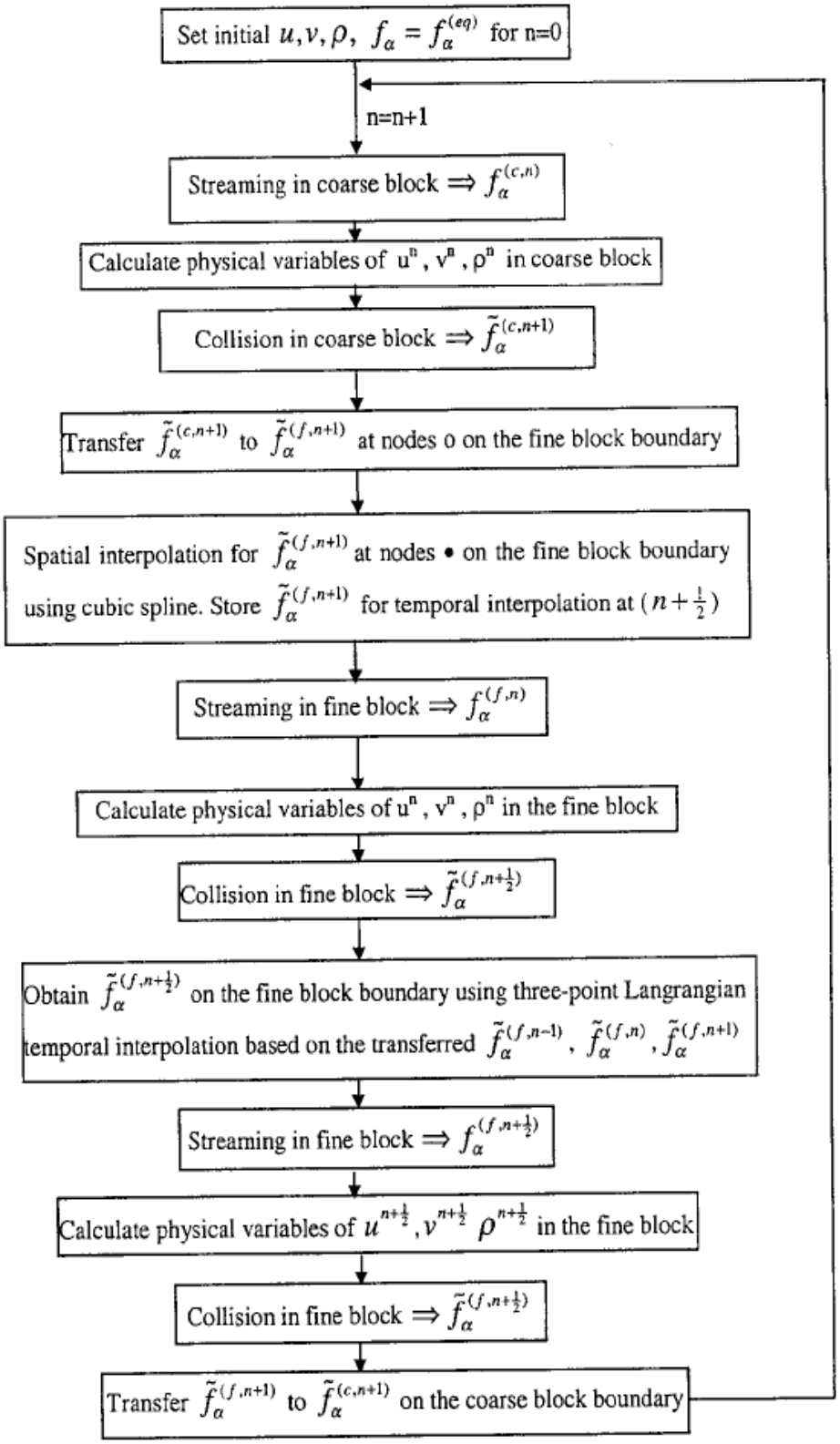

Figure 11: Flow of control for a multi-mesh code

Appendix B

Speed of sound

The concept of speed of sound shows up in LB methods when we try to derive the equilibrium distribution functions for finite and vanishing velocities.

The equilibrium distribution functions are given as, for example, see Nourgaliev et al (2003):

$$f_{a\neq 0}^{eq,k} = \rho_k \mathrm{w}_{i,k}\left[\frac{\mathrm{c}_{s,k}^2}{\mathrm{Y}_k^{(2)}} - \frac{\mathrm{v}^2}{2\mathrm{Y}_k^{(2)}} + \frac{\mathrm{e}_{ai}\mathrm{v}_i}{\mathrm{Y}_k^{(2)}} + \frac{\mathrm{e}_{ai}\mathrm{e}_{aj}\mathrm{v}_i\mathrm{v}_j}{2\mathrm{Y}_k^{(4)}}\right]$$

$$f_0^{eq,k} = \rho_k\left[1 - \frac{1-\mathrm{w}_{0,k}}{\mathrm{Y}_k^{(2)}}\mathrm{c}_{s,k}^2 - \frac{\mathrm{v}^2}{2}\left(\frac{\mathrm{Y}_k^{(2)}}{\mathrm{Y}_k^{(4)}} - \frac{1-\mathrm{w}_{0,k}}{\mathrm{Y}_k^{(2)}}\right)\right]$$

Subscript *k* is for the two fluids (alpha and beta).

$\mathrm{Y}_k^{(2)}$ and $\mathrm{Y}_k^{(4)}$ are given by :

$$\mathrm{Y}_k^{(2)} = \frac{3(1-\mathrm{w}_{0,k})}{5}\mathrm{c}^2 \tag{79}$$

$$\mathrm{Y}_k^{(4)} = \frac{(1-\mathrm{w}_{0,k})}{5}\mathrm{c}^4 \tag{80}$$

c is the *lattice velocity*.

$\mathrm{c}_{s,k}$ is the *pseudo-speed-sound*

$$\mathrm{c}_{s,k}^2 = \mathrm{Y}_k^{(2)} \tag{81}$$

Let $\frac{\rho_\alpha}{\rho_\beta} = r$

Also, $\mathrm{w}_{i,k}^{orth} = 4\mathrm{w}_{i,k}^{diag}$ (82)

$$\mathrm{w}_{i,k}^{diag} = \frac{1-\mathrm{w}_{0,k}}{20}$$

There are two ways in which we can proceed to find the equilibrium distribution functions for the two fluids:

A1. Pressure balance at the interface

$$\mathrm{P} = \rho_k \mathrm{c}_{s,k}^2 \quad (83)$$

At a flat interface,

$$\rho_\alpha \mathrm{c}_{s,\alpha}^2 = \rho_\beta \mathrm{c}_{s,\beta}^2$$

Therefore, $\mathrm{c}_{s,\alpha}^2 = \frac{\mathrm{c}_{s,\beta}^2}{r}$

So, $\mathrm{Y}_\alpha^{(2)} = \frac{\mathrm{Y}_\beta^{(2)}}{r}$

Or, $\mathrm{w}_{0,\alpha} = \frac{r-1+\mathrm{w}_{0,\beta}}{r}$ (84)

We are free to choose the speed of sound in the reference frame with the density equal to the lower density of the two fluids (β, by definition, is taken as the lighter of the two fluids).

$$\mathrm{c}_{s,\beta}^2 = \frac{1}{3} \quad (85)$$

This can be obtained by writing the Maxwell's equilibrium distribution function and taking the first four velocity moments.

c^2 is the *lattice speed* $\left(=\frac{\Delta x}{\Delta t}\right)$ which can be taken as '1' for both the fluids.

Using (79) and (85), we get:

$$\frac{3}{5}\left(1-w_{0,\beta}\right)=\frac{1}{3}$$

Or, $w_{0,\beta}=\frac{4}{9}$ (86)

Using (84), we get:

$$w_{0,\alpha}=\frac{4}{9}\left[\frac{9}{4}-\frac{5}{4r}\right]$$

Or, $w_{0,\alpha}=w_{0,\beta}\left[2.25-\frac{1.25}{r}\right]$ (87)

Using (82), (86), and (87) we get:

$$w_{i,\beta}^{diag}=\frac{1}{36} \quad (88)$$

$$w_{i,\beta}^{orth}=\frac{1}{9} \quad (89)$$

$$w_{i,\alpha}^{diag}=\frac{1}{36r} \quad (90)$$

$$w_{i,\alpha}^{orth}=\frac{1}{9r} \quad (91)$$

These choices of weight functions, derived from first principle, produce a stable interface with a finite density jump.

A2. Equal no-velocity equilibrium distribution functions for an interface with a finite density jump

Streaming step near the interface forces the two fluids to mix; for a stable interface, the single particle equilibrium distribution functions for vanishing velocities should be equal, or there will be unphysical momentum generation in the mixed region. Therefore:

$$\rho_\beta \mathrm{w}_{i,\beta}^{diag} = \rho_\beta \mathrm{w}_{i,\alpha}^{diag}$$

$$\rho_\beta \mathrm{w}_{i,\beta}^{orth} = \rho_\alpha \mathrm{w}_{i,\alpha}^{orth}$$

We can use the Maxwell's equilibrium distribution function for the lower of the two densities.

Therefore,

$$\mathrm{w}_{i,\beta}^{diag} = \frac{1}{36}$$

$$\mathrm{w}_{i,\beta}^{orth} = \frac{1}{9}$$

So, $\mathrm{w}_{i,\alpha}^{diag} = \frac{1}{36r}$

$$\mathrm{w}_{i,\alpha}^{orth} = \frac{1}{9r}$$

$\mathrm{w}_{0,k}$ can be calculated by using the following identity:

$$\mathrm{w}_{0,k} + 4\mathrm{w}_{i,k}^{diag} + 4\mathrm{w}_{i,k}^{orth} = 1$$

Plugging in the values of $\mathrm{w}_{0,k}$ in (79) and (81), we will obtain the expression for the speed of sound as:

$$c_{s,\beta}^2 = \frac{1}{3}$$

$$c_{s,\alpha}^2 = \frac{1}{3r}$$

Appendix C

Pressure Jump

Multiscale expansion of LBGK results in the following equations (Nourgaliev et al., 2003):

$$\partial_{\hat{t}}\hat{\rho} + \partial_{\hat{j}}\hat{\rho}\hat{\mathrm{v}}_j = 0 \tag{92}$$

$$\partial_{\hat{t}}\hat{\rho}\hat{\mathrm{v}}_i + \partial_{\hat{j}}\hat{\rho}\hat{\mathrm{v}}_i\hat{\mathrm{v}}_j = -\partial_{\hat{i}}\hat{p} + \partial_{\hat{j}}\left[\frac{\hat{\rho}}{\mathrm{Re}}\left(\partial_{\hat{j}}\hat{\mathrm{v}}_i + \partial_{\hat{i}}\hat{\mathrm{v}}_j\right)\right] + \frac{\hat{\rho}}{Fr}\hat{i}_i + \text{Non - linear deviations} \tag{93}$$

The ^ superscript denotes non-dimensionalized quantities. Re is the Reynolds number and Fr is the Froude number.

$\hat{i}_i$ is a unit vector specifying the orientation of the external body force.

Considering a case where the non-linear deviations, external body force, and variations in density are negligibly small, we obtain the following equation:

$$\partial_{\hat{t}}\hat{\mathrm{v}}_i + \partial_{\hat{j}}\hat{\mathrm{v}}_i\hat{\mathrm{v}}_j = -\frac{\partial_{\hat{i}}\hat{p}}{\hat{\rho}} + \frac{\partial_{\hat{j}}}{\mathrm{Re}}\left[\left(\partial_{\hat{j}}\hat{\mathrm{v}}_i + \partial_{\hat{i}}\hat{\mathrm{v}}_j\right)\right] \tag{94}$$

The external body force term is dropped even when there are body force terms at the interface due to the surface tension; the surface tension is an internal body force which sums up to zero if we consider the whole system together.

In dimensional form (94) gives:

$$\rho(\partial_i \mathrm{v}_i + \partial_j \mathrm{v}_i\mathrm{v}_j) = -\partial_i p + \mu\partial_j\left[\left(\partial_j \mathrm{v}_i + \partial_i \mathrm{v}_j\right)\right] \tag{95}$$

Define a unit normal vector at the interface (between the alpha and beta fluids; positive from beta to alpha) as:

$\vec{n} = \langle n_1, n_2 \rangle$

And a tangential vector as $\vec{t}$

Since the interface has no mass, the following conditions must be met:

1. The fluid velocity across the interface must be continuous.
2. The shear stress across the interface must be continuous.
3. The normal stress jumps by a finite quantity (proportional to the surface tension) across the interface.

The above conditions can be written in mathematical form as:

$$\left[\begin{pmatrix} \vec{n} \\ \vec{t} \end{pmatrix} (pI - \tau) \vec{n}^T \right] = (\sigma K) \tag{96}$$

$[A] = A_{alpha} - A_{beta}$

τ is the stress tensor.

Using the definition of τ, (96) can be written as:

$$\left[\begin{pmatrix} p \\ 0 \end{pmatrix} - \mu \begin{pmatrix} \vec{n} \\ \vec{t} \end{pmatrix} \begin{pmatrix} \nabla \mathrm{v}_1 \cdot \vec{n} \\ \nabla \mathrm{v}_2 \cdot \vec{n} \end{pmatrix} - \mu \begin{pmatrix} \nabla \mathrm{v}_1 \cdot \vec{n} & \nabla \mathrm{v}_2 \cdot \vec{n} \\ \nabla \mathrm{v}_1 \cdot \vec{t} & \nabla \mathrm{v}_2 \cdot \vec{t} \end{pmatrix} \cdot \vec{n} \right] = \begin{pmatrix} \sigma K \\ 0 \end{pmatrix} \tag{97}$$

This can be written as two separate jump conditions:

$$\left[p - 2\mu (\nabla \mathrm{v}_1 \cdot \vec{n}, \nabla \mathrm{v}_2 \cdot \vec{n}) \cdot \vec{n} \right] = \sigma K \tag{98}$$

$$\left[\mu (\nabla \mathrm{v}_1 \cdot \vec{n}, \nabla \mathrm{v}_2 \cdot \vec{n}) \cdot \vec{t} + \mu (\nabla \mathrm{v}_1 \cdot \vec{t}, \nabla \mathrm{v}_2 \cdot \vec{t}) \cdot \vec{n} \right] = 0 \tag{99}$$

Since the flow is viscous, the velocities are continuous:

$$[\mathrm{v}_1] = [\mathrm{v}_2] = 0 \tag{100}$$

As well as their tangential derivatives:

$$[\nabla \mathrm{v}_1 \cdot \vec{t}\,] = [\nabla \mathrm{v}_2 \cdot \vec{t}\,] = 0 \tag{101}$$

And the identity

$$(\nabla \mathrm{v}_1 \cdot \vec{n}, \nabla \mathrm{v}_2 \cdot \vec{n}) \cdot \vec{n} + (\nabla \mathrm{v}_1 \cdot \vec{t}, \nabla \mathrm{v}_2 \cdot \vec{t}\,) \cdot \vec{t}\, = \nabla \cdot \vec{\mathrm{v}} = 0 \tag{102}$$

can be used to obtain:

$$[(\nabla \mathrm{v}_1 \cdot \vec{n}, \nabla \mathrm{v}_2 \cdot \vec{n}) \cdot \vec{n}\,] = 0 \tag{103}$$

So equation (98) can be re-written as:

$$[p] - 2[\mu](\nabla \mathrm{v}_1 \cdot \vec{n}, \nabla \mathrm{v}_2 \cdot \vec{n}) \cdot \vec{n} = \sigma K \tag{104}$$

This is the correct pressure jump across an interface moving with a non-zero velocity.

$$[p] = \sigma K + 2[\mu](\nabla \mathrm{v}_1 \cdot \vec{n}, \nabla \mathrm{v}_2 \cdot \vec{n}) \cdot \vec{n} \tag{105}$$

This pressure jump can be seen as an interfacial body-force written in LB terms as:

$$g_i = 3\mathrm{w}_i \vec{\mathrm{e}}_i . ((\sigma K + S_1) n_1, (\sigma K + S_2) n_2) \tag{106}$$

Where:

$$(S_1, S_2) = 2[\mu](\nabla \mathrm{v}_1 \cdot \vec{n}, \nabla \mathrm{v}_2 \cdot \vec{n}) \tag{107}$$

References

Aidun CK, Lu Y. “Lattice-Boltzmann simulation of solid particles suspended in fluid.” Jounral of Statistical Physics 81 (1995): 49-61.

Aidun CK, Lu Y, Ding E. “Direct analysis of particulate suspensions with inertia using the discrete Boltzmann equation.” Journal of Fluid Mechanics 373 (1998): 287-311.

Alexander FJ, Chen S, Sterling JD. “Lattice Boltzmann thermodynamics.” Physical Review E 47 (1993): R2249-2252.

Aussillous P, Quere D. “Quick deposition of a fluid on the wall of a tube.” Physics of Fluids 12 (2000) : 2367-2371.

Bhatnagar PL, Gross EP, Krook M. “A model for collision processes in gases. I: small amplitude processes in charged and neutral one-component system.” Physical Review 94 (1954): 511-525.

Boghosian BM, Coveney PV. “Inverse Chapman-Enskog derivation of the thermohydrodynamics lattice-BGK model for the ideal gas.” International Journal of Modern Physics C 9 (1998): 1231-1245.

Broadwell JE. “Study of rarefied shear flow by the discrete velocity model.” Journal of Fluid Mechanics 19 (1964): 401-414.

Bretherton FB. “The motion of long bubbles in tubes.” Journal of Fluid Mechanics 10 (1961) : 161-165.

Buckmaster JD, Flaherty JE. “The bursting of two-dimensional drops in slow viscous flow.” Journal of Fluid Mechanics 60 (1973): 625-639.

Chen S, Doolen GD, Eggert K, Grunau D, Loh E Y. “Local lattice-gas model for immiscible fluids.” Physical Review A 43(1991): 7053-7056.

Chen H, Chen S, Matthaeus WH. “Recovery of the Navier-Stokes equations using a lattice-gas Boltzmann method.” Physical Review A 45 (1992): R5339-5342.

Frisch U, Hasslacher B, Pomeau Y. “Lattice-automata for the Navier-Stokes equation.” Physical Review Letters 56 (1986): 1505-1508.

Grunau D, Chen SY, Eggert K. “A lattice Boltzmann model for multiphase fluid flows.” Physics of Fluids A 5 (1993): 2557-2562.

Gunstensen AK, Rothman DH, Zaleski S, Zanetti G. “Lattice Boltzmann model of immiscible fluids.” Physical Review A 43(1991): 4320-4327.

Hardy J, de Pazzis O, Pomeau Y. “Molecular dynamics of a classical lattice gas: transport properties and time correlation functions.” Physical Review A 13 (1976): 1949-1961.

Higuera FJ, Jimenez J. “Boltzmann approach to lattice gas simulations.” Europhysics Letters 9 (1989): 663-668.

Higuera FJ, Succi S, Benzi R. “Lattice gas dynamics with enhanced collisions.” Europhysics Letters 9 (1989): 345-349.

Huang J, Xu F, Vallieres H, Feng DH, Qian YH, Fryxell B, Strayer MR. “A thermal LBGK model for large density and temperature differences.” International Journal of Modern Physics C 8 (1997): 827-841.

Inamuro T, Sturtevant B. “Numerical study of discrete-velocity gases.” Physics of Fluids 2 (1990): 2196-2203.

Inamuro T, Yoshino M, Ogino F. “A non-slip boundary condition for lattice Boltzmann simulations.” Physics of Fluids 7 (1995): 2928-2930.

Kang, Q, Zhang, D, Chen, S. “Immiscible displacement in a channel: simulations of fingering in two dimensions.” Advances in Water Resources 27 (2004): 13-22.

Lamb H. “Hydrodynamics.” Dover Publication, New York, 6^{th} edition (1945): 461.

Lavallee P, Boon JP, Noullez A. “Boundaries in lattice gas flows.” Physica D 47 (1991): 233-240.

McNamara GR, Zanetti G. “Use of the Boltzmann equation to simulate lattice-gas automata.” Physical Review Letters 61 (1988): 2332-2335.

McNamara GR, Garcia AL, Alder BJ. “Stabilization of thermal lattice Boltzmann models.” Journal of Statistical Physics 81 (1995): 395-408.

McNamara GR, Garcia AL, Alder BJ. “A hydrodynamically correct thermal lattice Boltzmann model.” Journal of Statistical Physics 87 (1997): 395:408.

Noble DR, Chen S, Georgiadis JG, Buckius RO. “A consistent hydrodynamic boundary condition for the lattice Boltzmann method.” Physics of Fluids 7 (1995):203-209.

Nourgaliev RR, Theofanous TG, Joseph DD. “The lattice Boltzmann equation method: theoretical interpretation, numerics and implications.” International Journal of Multiphase Flow 29 (2003): 117-169.

Pozrikidis C, Zhou H. “The flow of suspensions in channels: Single files of drops.” Physics of Fluids A 5 (1993): 311-324.

Qian YH, d'Humieres D, Lallemand P. "Lattice BGK models for Navier-Stokes equations." Europhysics Letters 17 (1992): 479-484.

Richardson S. "Two-dimensional bubbles in slow viscous flows." Journal of Fluid Mechanics 33 (1968): 475- 493.

Richardson S. "Two-dimensional bubbles in slow viscous flows 2." Journal of Fluid Mechanics 58 (1973): 115-127.

Rothman DH, Keller JM. "Immiscible cellular-automaton fluids." Journal of Statistical Physics 52 (1988): 1119-1127.

Saffman PG, Taylor G. "The penetration of a fluid into a porous medium or hele shaw cell containing a more viscous liquid." Proceedings of the Royal Society of London Series A, Mathematical and Physical Sciences 245 (1958): 312-329.

Shan X, Chen H. "Lattice Boltzmann model for simulating flow with multiple phases and components." Physical Review E 47 (1993): 1815-1819.

Shan X, Chen H. "Simulation of non-ideal gases and liquid-gas phase transitions by the lattice Boltzmann equation." Physical Review E 49 (1994): 2941-2948.

Skordos PA. "Initial and boundary conditions for the lattice Boltzmann method." Physical Review E 48 (1993): 4823-4842.

Somers JA, Rem PC. "Analysis of surface tension in two-phase lattice gases." Physica D 47 (1991): 39-46.

Sun C. "Adaptive lattice Boltzmann model for compressible flows: viscous and conductive properties." Physical Review E 61 (2000): 2645-2653.

Swift MR, Osborn WR, Yeomans JM. "Lattice Boltzmann simulation of non-ideal fluids." Physical Review Letters 75 (1995): 830-834.

Swift MR, Orlandi E, Osborn WR, Yeomans JM. "Lattice Boltzmann simulations of liquid-gas and binary fluid systems." Physical Review E 54 (1996): 5041-5052.

Taylor G. **"**The instability of liquid surfaces when accelerated in a direction perpendicular to their planes." Proceedings of the Royal Society of London Series A, Mathematical and Physical Sciences 201(1950): 192-196.

Wolfram S. "Cellular automaton fluids 1: Basic theory." Journal of Statistical Physics 45 (1986): 471-526.